ABSTRACT

BARUA, DIPAK. Deposition of metal and metal oxide thin films from metal organic precursors in supercritical carbon dioxide solution. (Under the direction of Gregory N. Parsons)

Thin films of metals and metal-oxides are deposited in batch (Chemical Fluid Deposition) and cyclic (Atomic Layer Deposition) processes from metal organic precursors in supercritical carbon dioxide solutions. New materials have been introduced in the deposition processes. Deposited films are analyzed in details in order to evaluate their quality and chemical composition. Analyzing techniques, X-ray photoelectron spectroscopy (XPS), ellipsometry, Fourier transform infrared spectroscopy (FTIR), atomic force microscopy (AFM), and auger electron spectroscopy (AES) are adopted to characterize the films. Capacitance-voltage measurements are performed to prove the device quality deposition of metal oxide films. The process establishes a new approach in metal oxide deposition, and controllable growth of metal and metal oxide films in supercritical carbon dioxide.

Deposition of Metal and Metal Oxide Thin Films from Metal Organic Precursors in Supercritical Carbon Dioxide Solution

by

Dipak Barua

A thesis submitted to the Graduate Faculty of

North Carolina State University

In partial fulfillment of the

Requirements for the degree of

Master's of Science

Chemical and Biomolecular Engineering

Raleigh, North Carolina

2005

Approved by:

Dr. Ruben G. Carbonell	**Dr. Carl Osburn**

Dr. Gregory N. Parsons

DEDICATION

This thesis is dedicated to my parents, Mr. Joysen Barua and Mrs. Jharna Barua, for their loving supports throughout my life.

BIOGRAPHY

Dipak Barua was born in Cox's bazar, a small city in Bangladesh. He was brought up in Chandpur, a different town in the same country, where he attended his high school (up to twelfth grade).In March 2002, he graduated with a bachelor of science degree in chemical engineering from Bangladesh University of Engineering and Technology, Dhaka, Bangladesh. In August 2003, he moved to United States in pursue of his graduate study at North Carolina State University in Raleigh, NC. He completed his Master's of Science in chemical engineering from North Carolina State University in May 2005, working under the direction of Dr. Gregory N. Parsons.

ACKNOWLEDGMENTS

I would like to thank first and foremost Dr. Gregory N. Parsons for his support, encouragement and guidance throughout the course of my research work. His invaluable direction as a mentor, teacher and a friend was essential at every step of this work. I am also grateful to him for giving me the opportunity to work in this exciting field of electronic materials.

I greatly appreciate my committee members, Dr. Ruben G. Carbonell and Dr. Carl Osburn, for their interest, comments and advice in my work. I am grateful to Dr. Ruben G. Carbonell for his invaluable suggestions and cooperation in this project from the very beginning. My thanks to Dr. Carl Osburn for his integrated circuit fabrication and design course, which gave me a broad overview about semiconductor processing and manufacturing.

My next thank goes to Dr.Theodosia Gougousi for her immense contribution to this project at its earlier stage. I am indebted to her for all her assistance, teaching and advice.

I am grateful to my fellow group members Jason M. Kelly, Kie Jin Park, David B. Terry, Changwoong Chu, Elisa Rosa and others for their assistance and ever needed help throughout my work. My thanks to Erin D. Young for her help in the experiments.

I am grateful to Dr. Genzer for allowing me using his laboratory facilities. My special thanks to Michael Tomilson and Rajendra Bhatt for training me the ellipsometer in their lab.

My special thanks to Kit Yeung, our instrument maker, for his help and suggestions in many cases.

I also acknowledge the financial support from National Science Foundation for carrying out my personal research traineeship in North Carolina State University.

TABLE OF CONTENTS

LIST OF TABLES vii

LIST OF FIGURES viii

CHAPTER ONE 1

1 INTRODUCTION 1

1.1 OVERVIEW OF THE THESIS 1

1.2 THIN FILM DEPOSITION: HIGH K DIELECTRICS AND GATE METALS . 2

1.2.1 High K Dielectric 2

1.2.2 Gate Metal and Metal-Oxides 3

1.3 SUPERCRITICAL CARBON DIOXIDE IN THIN FILM DEPOSITION 4

1.3.1 Chemical Fluid Deposition 5

1.3.2 Atomic layer deposition 6

1.4 OVERVIEW OF THE FOLLOWING CHAPTERS 7

1.5 REFERENCES 8

MY CONTRIBUTION TO THE FOLLOWING PAPER 9

CHAPTER TWO 10

2 Metal-oxide thin films deposited from metal organic precursors in supercritical CO_2 solutions. 10

2.1 INTRODUCTION 12

2.2 EXPERIMENTAL METHODS 14
2.3 RESULTS 16
I. Deposition of Al_2O_3 films 16
I.a Batch Deposition Method 16
I.b Cyclic Deposition Method 19
II. Batch Deposition of other Metal-Oxide Films 21
II.a Zr based films 21
II.b Ru based films 22
II.c Mn based films 23
2.4 DISCUSSION 24
2.5 CONCLUSIONS 25
2.6 ACKNOWLEDGEMENS 27
2.7 REFERENCES 28
CHAPTER THREE 46
3 Cyclic/Atomic Layer depositions of Metal-Oxide and Metal Thin Films from Metal Organic Precursors in Supercritical CO_2 Solution 46
3.1 INTRODUCTION 46
3.2 EXPERIMENTAL METHOD 48
3.3 RESULTS AND DISCUSSION 51
3.4 CONCLUSION 57
3.5 ACKNOWLEDGEMENTS 58
3.6 REFERENCES 59
CHAPTER FOUR 74
4.1 WORK SUMMARY 74
4.2 FUTURE WORK 75

LIST OF TABLES

Table 2.1 31

Table 3.1 List of metal and metal oxide films, precursors, experimental conditions and net results..... 63

Table 3.2 Number of deposition cycle, corresponding film thickness, and oxygen to aluminum atomic ratio in deposited films from three different sets of precursors. 64

LIST OF FIGURES

Figure 2.1 A schematic of the deposition system 32

Figure2.2 XPS survey scan for an Al based film deposited from $Al(acac)_3$ and H_2O_2 at at 120°C and 1700 psi . Peaks assigned to Al 2s, Al 2p , C1s and O1s core electrons can be distinguished. 33

Figure 2.3 High resolution scans for the (a) Al 2p, (b) C1s and (c) O1s peaks for XPS survey scan for an Al based film deposited from $Al(acac)_3$ and H_2O_2 at 120°C and 1700 psi on Si substrates with native oxide. From the location and width of the peaks we conclude that the film is a mixture of Al_2O_3, Al(OH)O and Al-carbonate. 34

Figure 2.4 Transmission IR spectrum for an Al-based film deposited from $Al(acac)_3$ and H_2O_2 at 120°C and 1700 psi on Si substrates with native oxide. Curve (i) shows a measurement taken after film deposition and curve (ii) shows a spectrum taken after the film was annealed at 600°C in N_2 for 5 min. Spectrum (i) exhibits features at 1200-1700 cm^{-1} associated with several carbonate species. The broad peak at 3000-3600 cm^{-1} is due to the O-H stretching modes of both undissociated H_2O molecules and surface H-bonded OH species. Al-O bonding is detected by the borad peak at 400-800cm^{-1}. Mild anneal result in the disappearance of the IR signature of the carbonates and hydroxides. 35

Figure 2.5 Transmission IR spectrum for an Al-based film deposited from $Al(hfac)_3$ and H_2O_2 at 130°C and 2500 psi. The spectrum shows features compatible with the presence of H_2O in the film (3600-3000 cm^{-1}) and Al-O bonding (850-500cm^{-1}). Well resolved peaks at 1700cm^{-1} and 1300-1150cm^{-1} are attributed to the presence of carbonate type and C-F

bonding in the film. A mild anneal for 10 min at 600°C in N_2 removes most of the IR signature of these impurities, and reinforces the Al-O peak. 36

Figure 2.6 Frequency dependence (a) and hysteresis (b) of the C vs. V measurements for Al-based film deposited from $Al(acac)_3$ and H_2O_2 at 80°C , 2060 psi and annealed at 600°C in N_2 for 10 min. Change of frequency from 1MHz to 100 KHz does not change the shape of the curve substantially indicating good quality interface. However, the hysteresis is quite large ~500 mV. 37

Figure 2.7 High resolution XP scans for the (a) Al 2p, (b) C1s, and (c) O1s peaks for two aluminum based films deposited via reagent cycling. Both films were deposited at 120°C, and 1600 psi. Film marked HP was deposited form $Al(acac)_3$ and H_2O_2, while film TBP was deposited from $Al(acac)_3$ and tert-butyl peracetate 38

Figure 2.8 High resolution XP scans for the (a) Zr 3d, (b) C1s, and (c) O1s peaks for a Zr based film deposited from $Zr(acac)_4$ and tert-butyl peracetate at 150°C, and 1700psi. The film composition can best be described a hydroxycarbonate. 39

Figure 2.9 XP survey spectrum for a Ru based film deposited from $Ru(tmhd)_3$ and H_2O_2 at 150°C, 3600 psi. The presence of the Ru 3d and Ru 3p peaks verify the deposition of a Ru-based film on Si substrate. 40

Figure 2.10 High resolution XP scans for the (a) Ru 3d- C1s, and (b) O1s peaks for a Ru based film deposited from $Ru(tmhd)_3$ and H_2O_2 at 150°C, 3600 psi. The film contains a mixture of Ru oxides and possibly carbonates and hydroxides. 41

Figure2.11 XP survey spectrum for a Ru based film deposited from ruthenocene and H_2O_2 at 130°C, 3120 psi. The presence of the Ru 3d and Ru 3p peaks verify the deposition of a Ru-based film on Si substrate. 42

Figure2.12 High resolution XP scans for the (a) Ru 3d- C1s, and (b) O1s peaks for a Ru based film deposited from ruthenocene and H_2O_2 at 130°C, and 3120 psi. The film contains a mixture of Ru oxides and possibly carbonates and hydroxides. 43

Figure2.13 XP survey spectrum for a Mn based film deposited from $Mn(hfac)_3$ and H_2O_2 at 150°C and 3500 psi. Fluorine from the precursor is observed in the film. 44

Figure2.14 High resolution XP scans for the (a) C1s, (b) O1s and (c) Mn 2p peaks for a Mn based film deposited from $Mn(hfac)_3$ and H_2O_2 at 150°C and 3500 psi. The highlighted area on plots b and c show the range of binding energies available to O 1s and M2p electrons due to the large number of oxidation states available to the Mn atoms. The film contains a mixture of Mn oxides with carbonates and hydroxides. 45

Figure 3.1 Schematic diagram of the experimental set-up 65

Figure 3.2 Ellipsometric thickness data for Al-based film deposited from $Al(hfac)_3$-H_2O_2 at 100°C and ~2000 psi on Si(100) with native oxide. Figure shows linear growth behavior. Longer precursor time shows high rate of film growth. For same precursor exposure time (30 seconds), different growth rates are observed for two different sample orientations. 66

Figure 3.3 AFM image of Al-based film deposited in 23 cycles from $Al(hfac)_3$-H_2O_2, at 100°C and ~2000 psi. JTB treated native Si(100) is used as the substrate. The RMS value for

the film is ±2.3 nm while the ellipsometric thickness is 117 Å. The gray scale of this image spans 100 Å from dark to light and each unit in the z-direction corresponds to 50 nm……..67

Figure 3.4 High-resolution XPS peaks for I. Al 2p, II. O 1s, and III. C 1s deposited from a)$Al(hfac)_3$-H_2O_2 at 100°C,~2000 psi, b)$Al(acac)_3$-H_2O_2 at 120°C, ~1600 psi, and c) $Al(acac)_3$-TBP at 120°C and ~1600 psi. Native Si(100) is used as the substrate. Comparative chemical states are evaluated from the relative peak positions for the different sets of precursors. 68

Figure 3.5 High resolution XP-Spectra for a) C1s, b) Pd 2p,and c) O1s for palladium film deposited from $Pd(hfac)_2$-H_2 in 20 cycles. Native Si(100) is used as the substrate. Deposition temperature is 70°C and pressure ~2000 psi. Ligand and precursor derived contamination from fluorine, carbon and oxygen is anticipated. 69

Figure 3.6 Comparative XPS peaks for Pd3d and Si 2p.Palladium film is deposited from $Pd(hfac)_2$-H_2 in different two different number of cycles. Si(100) with native oxide is used as the substrate. The large difference in Pd3d to Si2p peak-height ratio in two cases indicates multilayer film growth in each cycle..... 70

Figure 3.7 AES survey spectra for RuO_x film deposited from ruthenocene ($RuCp_2$) and H_2O_2 in 10 cycles. Reaction temperature is 100° C and pressure ~2000 psi. Si(100) with native oxide is used for deposition. The inset shows high- resolution peak for Ru LMM. ... 71

Figure 3.8 High resolution XP-spectra showing a) Ru3p and b) Si 2p peaks for the RuOx films deposited on chemically oxidized surface of Si(100) at 200°C and ~1500 psi. The attenuating intensity of Si 2p signal indicates growing film thickness with increasing number of deposition cycle..... 72

Figure 3.9 AFM images of Ru/RuOx film deposited from $RuCp_2$ and H_2O_2 at 200°C and ~1500 psi: a) 8 cycles, b)20 cycles, and c)30 cycles. Chemically oxidized Si(100) was used for the deposition. Figure shows increasing surface roughness with increasing number of deposition cycles. Change in interface morphology indicates non-ideal ALD growth. 73

CHAPTER ONE

1 INTRODUCTION

1.1 OVERVIEW OF THE THESIS

At the end of the twentieth century, the semiconductor industry went through a technology boom and an unprecedented progress was achieved in this field. The advent of high technology processes and newer inventions lead to an exponential increase in quality and quantity in semiconductor device processing and characterization. In spite of this revolution, the basic and key issues for microfilm deposition, the core of semiconductor processing, remained unresolved, and imposing a great challenge against this on going momentum. Therefore, newer approaches in thin film deposition processes are essential at this moment.

Current thin film deposition techniques are based on high vacuum processes which involve several limitations such as high process temperature, low precursor volatility, thermodynamic instability at heterogeneous interface, non-conformal deposition on high aspect ratio surface, etc. In order to overcome these limitations, extensive researches are now focused on exploring and utilizing the possibilities of different deposition techniques such as chemical vapor deposition (CVD), plasma enhanced chemical vapor deposition (PECVD), photon assisted chemical vapor deposition (PACVD), atomic layer deposition (ALD), etc. In addition to these better-known high-vacuum processes, supercritical carbon dioxide (Sc CO_2) based deposition of microfilm is at its infantry and almost unexplored. My research in the Department of Chemical and Biomolecular Engineering of North Carolina State University is to develop a supercritical carbon dioxide based deposition system and explore its potential or low temperature deposition of ultra-thin, high k dielectric materials and gate metals using

metal organic precursors. The goal of this dissertation is to present a rigorous analysis of the deposited film in quest of the following:

1. Viability of supercritical carbon based deposition process for metal and dielectric deposition in parallel to its high vacuum counterparts.
2. Potential application of supercritical carbon dioxide for film growth in atomic layer deposition (ALD) process.
3. Evaluation of deposited films in terms of their chemical composition and film purity

A Sc CO_2 based high pressure deposition system has been developed and used to deposit different metal oxides (aluminum oxide, zirconium oxide, manganese oxide, ruthenium oxide, and yttrium oxide), and metals (palladium and ruthenium) from metal organic precursors in Sc CO_2 solution. Experiments are conducted in two different modes, chemical fluid deposition (CFD) [1] and atomic layer deposition (ALD).[2] New sets of materials are introduced in the deposition processes and device quality metal oxide films are obtained from the CFD process. The ALD process has been proven to give tunable film thickness although this process does not obtain atomically controlled growth. Both processes show low temperature (70-200°C) deposition although film composition and surface morphology are not up to expectation in many cases.

1.2 THIN FILM DEPOSITION: HIGH K DIELECTRICS AND GATE METALS

1.2.1 High K Dielectric

Silicon dioxide (SiO_2) has been used as the gate dielectric in metal-oxide-semiconductor (MOS) devices for past 30 years. Rapid reduction in device dimension is a challenge for SiO_2 gate dielectric in future MOS devices. As devices dimension goes smaller,

it becomes necessary to reduce the thickness of the gate oxide in order to meet the target device capacitance. The capacitance of a dielectric can be expressed as $C = \varepsilon_r\varepsilon_0/t_{ox}$, where dielectric constant, $k=\varepsilon_r$, t_{ox} is the gate oxide thickness and C is the gate capacitance per unit area. Reduced thickness leads to an exponential increase in electron tunneling through gate oxide. Therefore, a replacement of SiO_2 with some high dielectric constant material is necessary for advanced MOS devices. A high dielectric constant would allow a thicker film in place of SiO_2 thereby minimizing the leakage current but still giving the same capacitance. Metal oxides such as, aluminum oxide, (Al_2O_3), tantalum oxide (Ta_2O_5), zirconium oxide (ZrO_2), hafnium oxide (HfO_2), titanium oxide (TiO_2), and $SrTiO_3$, yttrium oxide (Y_2O_3), with a k value ranging 10-40 [3], are potential candidates for high k gate dielectric applications. In this work, we introduced the Sc CO_2 based deposition of high k metal oxides for the first time.

1.2.2 Gate Metal and Metal-Oxides

In current CMOS devices, highly doped p-type and n-type polysilicon are used as gate electrodes on top of the gate dielectric layers. The high resistance of the polysilicon-gate and its dopant depletion is a significant issue against its use for sub-100 nm scale semiconductor devices. The resistance of a polysilicon gate can be reduced by increasing its dopant concentration although the maximum concentration of the dopant is limited by its solubility in polysilicon. Further, high doping can enhance boron penetration into the dielectric underneath which degrades the device performance. The dopant depletion in polysilicon increases the equivalent gate-oxide thickness, which in turn reduces the effective capacitances per unit area. For these reasons, metal gates are now being considered as a replacement of polysilicon gates in future CMOS devices. Metal electrodes would impose a

lower contanct resistance than the polysilicon in smaller devices. Also high k dielectric layers are now being considered for gate-oxide applications, which seem to be more compatible with a metal than with polysilicon. Two different type metals are now being considered for gate electrode applications: high work function metals in place of a p-doped polysilicon and low work function metals in place of an n-doped polysilicon. In this study we focused on two high work function metal/metal oxide (palladium and ruthenium oxide), both having a work function close to 5.0 eV. Although not a metal, ruthenium oxide is a conductor and therefore considered as a potential candidate for gate electrode applications.

1.3 SUPERCRITICAL CARBON DIOXIDE IN THIN FILM DEPOSITION

Supercritical fluids have been widely used in extraction, polymerization and separation processes.[4, 5] Recent studies open up different sectors of semiconductor industry for potential applications of Sc CO_2. The tunable solvation energy of Sc CO_2 and its unique combination of high density and gas-like viscosity make it a lucrative alternative for currently used aqueous and organic solvents in microelectronics processes, such as etching, cleaning, drying, and resist development, deposition, and stripping, etc.[6,7, 8] Thin film deposition is a recent addition to these versatile applications of Sc CO_2.

Supercritical carbon dioxide possesses the beneficial aspects of both liquid and gas. Its high density facilitates the dissolution of metal organic species, and removal of reaction byproducts and impurities from the deposition surface. The low viscosity and high diffusivity of Sc CO_2 is important in minimizing the mass transport limitations in severely constrained surface geometries. Zero surface tension of Sc CO_2 provides it with the ability to permeate and wet the deepest and narrowest trenches on the deposition surface. The high solubility of metal-organic precursors in Sc CO_2 can ensure a high flux on to the deposition surface

thereby enhancing the film growth rate. Supercritical carbon dioxide is expected to broaden the range of applicable precursors since the process is not limited by the precursor volatility. Its non-toxic nature, amenable operating conditions and low cost of production make it a unique choice among all other supercritical fluids.

In high vacuum processes, the kinetics of surface reaction including surface adsorption/desorption of chemical species, oxidation, and reduction are driven by thermally heating the solid substrate. The enhanced solvation energy of Sc CO_2 can be a supplement for a part of this thermal energy and minimize the deposition temperature thereby. Effective use of solvation force effects is well established in electroplating and electroless deposition processes.

1.3.1 Chemical Fluid Deposition

Hansen and his coworkers, in 1992, first demonstrated Sc CO_2 assisted deposition of Indium thin film from thermal decomposition of Indium acetylacetonate at 600°C.[9] Later, in 1999, Watkins and his coworkers deposited platinum thin film from hydrogen- reduction of a platinum metal organic precursor in supercritical carbon dioxide at a temperature at 80ºC.[1] The process, named chemical fluid deposition (CFD) by Watkins and his coworkers, is a batch deposition process where the dissolved species in Sc CO_2 react and form the metal film on the deposition surface. To date, deposited films by CFD include Pt, Pd, Ru, In, Rh, Cu, Au, and Ag. We introduced the deposition of metal oxides such as, Al_2O_3, ZrO_2, RuOx, Y_2O_3 and MnO_2 by this process.

Chemical fluid deposition seems to be a promising alternative for CVD and electroless deposition processes since it combines the beneficial aspects of both the processes

while eliminating their limitations. CVD process is restricted by a few volatile precursors and high reaction temperatures. Low volatility of precursors in CVD results in low gas phase concentration, which reduces mass transfer in tortuous geometries. High processing temperatures in CVD induce thermal and mechanical stresses, internal diffusion, and interlayer reaction. Recent development of few metal organics and fluorinated precursors allows low temperature MOCVD, but lowering of reaction temperature further exacerbates film quality since surface desorption of reaction byproducts is kinetically driven by surface heating. Use of liquid solvents in electroless deposition facilitates dissolution of chemical species although high viscosity, high surface tension and low molecular diffusion in liquid phase inhibit mass transport in constrained areas of the deposition surface.

1.3.2 Atomic layer deposition

Atomic layer deposition was first introduced by Suntola in 1970. The process involves an alternate exposure of the substrate to reactants and intermediate purging of the reactor after each exposure. During each exposure, the reactant species react with the surface to form a chemisorbed monolayer. Therefore, film growth proceeds in a self limiting fashion with a maximum thickness of one monolayer in each cycle. The thickness of ultra thin film can be tuned by varying the number of deposition cycles. Film growth takes place in atomic level on the interface while not affecting the bulk of the substrate. Low temperature deposition, multi-level processing, better film quality and uniformity over large area are the other benefits of ALD.

No previous work has been reported on supercritical carbon dioxide based ALD process. In this study, we introduced the supercritical carbon dioxide based ALD for the first time. Experiments were carried out in a typical ALD mode with alternate precursor

exposures and intermediate flushing of the reaction cell with liquid/Sc CO2. Deposited films by this process include aluminum oxide, palladium and ruthenium/ruthenium oxide.

1.4 OVERVIEW OF THE FOLLOWING CHAPTERS

Chapter two focuses on analyzing the chemical composition of different metal-oxide films deposited from metal organic precursors. Also it compares the effect of different materials used in the process. Detailed analysis leads to the fact that in deposited metal oxides, the metals stay in multiple oxidation states. Formation of carbonates having different metal content is observed depending on the oxidant used in the process. Post deposition annealing has a significant effect on film composition. Electrical measurement proves device quality deposition of metal oxide.

Chapter three aims at the atomic layer deposition process in supercritical carbon dioxide medium. Detailed analyses are made to evaluate the process viability. Linear film growth with deposition cycles has been established although atomic level growth is not proved in this case. Compositional analyses are performed on the aluminum oxide and palladium films. Surface morphologies of metal-oxide and metal films are evaluated to justify this process.

1.5 REFERENCES

1. James J. Watkins, Jason M. Blackburn and Thomas J. McCarthy, "Chemical Fluid Deposition: Reactive Deposition of Platinum Metal from Carbon Dioxide Solution, *Chemistry of Materials* **11**, 213-215 (1999)

2. Tuomo Suntola, Jaakko Hyvarinen, "ATOMIC LAYER EPITAXY", Annual Review of Materials Science 15, 177-195(1985)

3. E.P. Gusev, E. Cartier, D.A. Buchanan, M. Gribelyuk, M. Copel, H. Okron-Schmidt, C.D'Emic, "Ultrathin high-K metal oxides on silicon: processing, characterization and integration issues, Microelectronic Engineering 59, 341-349 (2001)

4. M. Angela, A. Meireles, "Supercritical extraction from solid: process design date (2001-2003)", Current Opinion in Solid State and Materials Science 7, 321-330 (2003)

5. Andrew I. Cooper, "Polymer synthesis and processing using supercritical carbon dioxide", Journal of Materials Chemistry 10, 207-234(2000)

6. Charles A. Jones, III, Dongxing Yang, Eugene A. Irene, Stephen M. Gross, Mark Wagner, James DeYoung, and Joseph M. DeSimone, "HF Etchant Solutions in Supercritical Carbon Dioxide for "Dry" Etch Processing of Microelectronic Devices", Chemistry of Materials 15, 2867-2869(2003)

7. Gina L. Weibel, Christopher K. Ober, "An overview of supercritical CO2 application in microeletronics processing", Microelectronic Engineering 65, 145-152 (2003)

8. David J. Mount, Laura B. Rothman, Raymond J. Robey, Mir K. Ali, "The technology behind cleaning with supercritical fluids", Solid State Tchnology, 103-106(2002)

9. Brian N. Hansen, Brooks M. Hybertson, Robert M. Barkley, and Robert E. Sievers, "Supercritical Fluid Transport-Chemical Deposition of Films", *Chemistry of Materials* **4**, 749-752 (1992)

MY CONTRIBUTION TO THE FOLLOWING PAPER

The following paper, written by Dr. Theodosia Gougousi, includes my name as the second author, reflects my participation in some of the experiments and analytical measurements. Dr. Theodosia Gougousi was working as a post doctorate fellow here, and she was conducting the research on this project. During the later stages of her work, I joined this project and I was working with her as an assistant. Some of the experiments were done before I joined here, although I took part in the analytical measurements for those experiments (C-V measurement, Ellipsometry, FTIR) as per her guidance.

The data that I acquired by analytical measurements include figure 2.4 (FTIR), 2.5 (FTIR), 2.6 (Capacitance-Voltage), ellipsometry (we both did it together for several samples).

For the XPS measurements, I was with her during the XPS operation and data collection, although I could not take part actively because of my technical ignorance of XPS at that time.

During the experiments, I was with Dr. Theodosia Gougousi and I was learning the process from her. My other contribution to the process is to build up the temperature controlling system for the experimental set-up.

CHAPTER TWO

2 Metal-oxide thin films deposited from metal organic precursors in supercritical CO_2 solutions.

Theodosia Gougousi,[*†] *Dipak Barua, Erin D. Young,*[‡] *and Gregory N. Parsons*

Department of Chemical and Biomolecular Engineering

North Carolina State University

Raleigh, NC 27695

RECEIVED DATE

ABSTRACT: Metal Oxide thin films, including Al_2O_3, ZrO_2, MnO_x and RuO_x were deposited on Si(100) substrates using metal-organic and precursors and oxidizing agents dissolved in liquid and supercritical CO_2 at pressures ranging from 1600 to 3600 psi using a hot wall reactor. Precursors included $Al(acac)_3$, $Al(hfac)_3$, $Zr(acac)_4$, $Mn(hfac)_4$ and

* to whom correspondence should be addressed. E-mail: gougousi@umbc.edu

† Current address: Department of Physics, University of Maryland, Baltimore County, 1000 Hilltop Circle, Baltimore, MD 21250

‡ Current address: Department of Chemical Engineering, University of Virginia, 102 Engineers' Way P.O. Box 400741, Charlottesville, VA 22904-4741

$Ru(tmhd)_4$. Aqueous H_2O_2 (30% weight) and tert-butyl-peracetate (50% in mineral spirits) solutions were used as oxidizing agents. Growth was investigated at temperatures between 80°C and 200°C and compositional analysis of the films by X-ray photoelectron spectroscopy, Auger electron spectroscopy and infrared transmission confirmed metal oxide formation, although carbon content can be large under some conditions. Capacitance vs. voltage analysis for the Al_2O_3 films annealed after deposition show that the films have good dielectric properties. Utilization of supercritical carbon dioxide may provide an avenue for the low temperature deposition of high quality metal-oxide thin films.

KEYWORDS: supercritical fluids, thin film deposition, high-k dielectrics, metal-oxide films, Al_2O_3, ZrO_2, MnO_x, RuO_x

2.1 INTRODUCTION

In most deposition and etching processes used for nano-electronic device fabrication, kinetically controlled reactions, such as reactant adsorption, surface oxidation (or reduction), and by-product removal are driven by energy delivered to the surface via substrate heating. Other means for energy delivery includes plasmas and photon or ion bombardment, and often the specific effects of these energy delivery approaches result to severe damage to the deposited material. Another means to deliver energy is the use of solvation forces. These forces are not commonly applied in thin film processing, but they could be utilized to help enhance and expand the range of materials and conditions over which thin film deposition and etching processes could be applied. In principle, energy associated with reactant or product solvation or dissolution could be used to promote a desired reaction step. For example, additional energy provided by solvation forces could enable deposition of metals at very low temperatures on organic surfaces, where the solvent strength and structure is designed to remove the unwanted metal-organic ligand without affecting the molecular growth surface. Eventually, solvent assisted deposition could provide a means to stabilize desired reaction intermediates during deposition, to enable tuning of the structure and composition of the deposited film. Solution-based processes that involve solvation force effects are widely used for electroplating or autocatalytic (electroless) deposition [1], [2], and other applications, but these approaches are generally not amenable to a wide range of materials.

The enhanced solvent characteristics of supercritical fluids [3] have been widely utilized for extraction, separation, polymerization,[4] and other chemical processes including metal thin film deposition.[5], [6], [7] Supercritical fluids are attractive solvents because

they provide high solubility of many species, due in part to high fluid density, and they maintain beneficial aspects of gases, including low viscosity and high diffusivity.[3] For example, the density of supercritical CO_2 (critical temperature 31°C and critical pressure $7.4x10^6$ Pa) can exceed that of liquids, but the diffusivity of species dissolved in CO_2 is between that of species in liquid (~10^{-5} cm^2/s) and gases (~1 cm^2/s) under typical process conditions. Supercritical CO_2 can suspend a significant density of molecular H_2, and the relatively high diffusivity can therefore enable a high flux of hydrogen or other soluble reactive species to be delivered to a deposition surface [7], [8]. For these studies, supercritical CO_2 was used because it has an easily accessible supercritical point, and is safe to work with.

Metal oxide materials are widely used in electronic devices for applications including high dielectric constant insulators in transistor structures [9], magnetic tunnel junctions in spintronic devices[10], as well as for optical coatings, barrier layers, and catalytic materials. In this article, we demonstrate preparation of metal oxide films from metal alkoxide precursors and oxidizing agents dissolved in liquid and supercritical carbon dioxide.

In most solvent-based thin film deposition processes, the substrate is exposed simultaneously to the precursor and oxidants (or reductants), leading to continuous growth, where the rate is determined by precursor supply or the rate of surface kinetic rate processes.

An alternate approach, widely used in vapor-phase deposition, is to supply reactants sequentially, where individual adsorption and reaction steps are controlled individually. Atomic layer deposition, for example, involves sequential reactant exposure where each reaction step is self-limiting. In this article, we demonstrate both continuous and time-

sequenced chemical deposition of metal oxide films from precursors dissolved in liquid or supercritical CO_2.

2.2 EXPERIMENTAL METHODS

The films were deposited on native oxide or H-terminated Si (100) surfaces. Both types of substrates were prepared by wet cleaning (JTB-100 Baker clean), deionized water rinse and blown dry with N_2. For the H-terminated surfaces the dry substrates were dipped in Buffered Oxide Etch (BOE) typically for 5 to 10s until they appeared dewetted upon removal. The precursors were purchased from commercial sources (Sigma-Adrich and Strem Chemicals) and used without further treatment. Coleman grade CO_2 with a 99.99% purity was used for all the experiments.

All films were deposited in a homemade high-pressure ~20 mL stainless steel cell with sapphire windows. Two different deposition methodologies were explored: 1) batch processing, where all reactants were introduced to the deposition vessel simultaneously; and 2) cyclic processing, where reactants were introduced in a sequential repeated time sequence to build films layer-by-layer. A piece of pretreated Si was placed inside the cell along with a known mass, usually 0.3-0.5 wt.%, of the relevant precursor. The cell was then sealed and heated to 45°C using resistive heaters. Once the temperature of the cell equilibrated, usually within 15-20min, the cell was filled with pressurized CO_2 from an ISCO 260D syringe pump through a high-pressure manifold. Then the temperature was raised to the desired reaction temperature and the precursor was allowed to dissolve. For some of the fluorinated metal organic precursors this was accomplished within a few minutes and the dissolution could be monitored through the window. For less soluble precursors such as the acetylacetonates the precursors were allowed about 30 min to saturate the solution. Then ~0.3ml of the oxidizer

solution was injected inside the high-pressure manifold and CO_2 from the syringe pump was used to push it inside the cell. Two oxidizers were tested in the course of this work; a 30% aqueous solution of H_2O_2 and a 50% solution of tert-butyl peracetate in mineral spirits. The H_2O_2 has very poor solubility in sc CO_2 while tert butyl peracetate has very high solubility. In both cases the oxidizer to precursor molar ratio was approximately 50x, and the reagents were permitted to react for 30 – 90 min. The experimental set up is shown on Fig 2.1 and it follows the technique developed by Watkins et al.

For the cyclic deposition process the substrate was exposed sequentially to the precursor and the oxidizer imitating the Atomic Layer Deposition technique (ALD) developed for vacuum based thin film deposition. For that purpose a precursor solution in supercritical carbon dioxide was prepared in a high pressure generator (~60 mL). The alternating exposure can be described as follows: Initially, the reaction cell was purged and then pressurized with CO_2 at ~1500psi at the desired reaction temperature. Then, a small amount of the oxidizer solution was admitted in the reaction cell. For H_2O_2 the fluid was injected as described above for the batch process. Tert-butyl peracetate is soluble in sc CO_2 and a solution in supercritical carbon dioxide (~60°C) was prepared in a large volume (~100mL) high-pressure cell. The oxidizer solution was permitted to equilibrate and saturate the substrate surface for 3-5 min. Then the cell was flashed slowly, using a continuous CO_2 stream to avoid oxidizer precipitation on the substrate. From atmospheric pressure the cell was pressurized again to ~1500 psi and the precursor solution was injected in the cell. Substrate exposure times were comparable to the oxidizing step. Following exposure the cell was evacuated and the process repeated. The duration of each cycle was between 20 and 45 min.

The samples were characterized using X-ray Photoelectron Spectroscopy (XPS), transmission Fourier Transform Infrared Spectroscopy (FTIR), and capacitance vs. voltage measurements (C-V). The XPS measurements were performed with a Riber LAS3000 (MAC2 analyzer, Mg Kα hv=1253.6 eV, non-monochromatic X-ray source) at 75º take-off-angle with 0.1eV step size. We compensated for sample charge effects by setting the adventitious C 1s peak to a binding energy of 285.0 eV. A ThermoNicolet IR bench equipped with a Deuterated Tri-Glycine Sulfate detector (KBr beamsplitter) was used in the transmission mode and for a typical spectrum we collect 256 scans at 4 or 8 cm^{-1} resolution. The instrument was purged using purified air with low concentrations of moisture and CO_2. A background spectrum was collected after each measurement using a substrate fragment that originates from the same wafer as the deposited substrate.

For electrical analysis aluminum top and back-contacts were formed by resistive-heating evaporation using shadow masks. Capacitances vs. voltage measurements were performed with an HP 4284A impedance meter at 1MHz. Typical capacitor area was ~$4.3x10^{-4}cm^2$. Flatband voltage (VFB) and equivalent oxide thickness (EOT) were obtained by processing the C-V characteristics with the NCSU C-V program that includes corrections for the quantum mechanical effects.[9]

2.3 RESULTS

I. Deposition of Al_2O_3 films

I.a Batch Deposition Method

Aluminum oxide films were deposited on Si substrates via both the batch and the cyclic deposition approach using aluminum acetylacetonate ($Al(acac)_3$) and its fluorinated

equivalent, aluminum hexafluoroacetylacetonate ($Al(hfac)_3$), as precursors. Figure 2.2 shows the XPS survey spectrum for a film that was deposited using the batch approach on native oxide Si substrate at 120°C and 1700 psi using $Al(acac)_3$ and H_2O_2. In the spectrum, features associated with the O1s, C1s and Al 2s and 2p core electron are observed confirming the presence of these elements in the film. Si peaks are not visible indicative of film at least 50Å in thickness. For more information regarding the bonding environment in the film, high resolution scans of the Al 2p, C1s and O1s peaks are presented in Figure 2.3. In the more detailed Al 2p spectral region shown in Fig 2.3(a) a broad feature located at 74.3 eV is observed. The width of the peak suggests that Al is present in the film in more than one oxidation state. The $2p_{3/2}$ electrons from elemental Al have a binding energy of 72.8 eV[11], while $2p_{3/2}$ electrons from Al bound to O in Al_2O_3 have a binding energy of 74.6 eV [12]. The Al $2p_{3/2}$ electrons in AlO(OH) have a binding energy of 76.7eV[13], and range[14],[13] from 74.3 eV to 75.9 eV in $Al(OH)_3$. The high-resolution scan for the O1s region (Fig. 2.3c) shows a fairly broad peak at 532.4 eV, also consistent with a range of binding environments. The O1s electron binding energy for Al_2O_3 is 531.4 eV [15], which is similar to the O1s binding energy for $Al(OH)_3$ at 531.53eV[16] and that for AlO(OH) at 531.5.[14] The O1s electrons in carbonate species are also known to have binding energies[17], [18] around ~532 eV. The C1s high-resolution scan shown on Fig. 2.3b confirms the presence of bound carbon atoms in the film. Two peaks are clearly resolved; the one at 285 eV can be ascribed to adventitious C while the peak at 289.5 eV is indicative of C bonded to a more electronegative element, probably oxygen.

Transmission infrared spectroscopy can be used to confirm the presence of carbonate species in the film. Figure 2.4 shows the infrared spectrum for an Al_2O_3 film prepared under similar conditions (curve i). The 1200-1700 cm^{-1} spectral range is associated with

absorptions from several carbonate species. The broad peak at 3000-3600 cm^{-1} is due to the O-H stretching modes of both undissociated H_2O molecules and surface H-bonded OH species.[19] Finally the broad peak at 400-900 cm^{-1} indicates complex Al-O vibrations due to Al atoms in either tetrahedral or octahedral coordination surrounded by cubic close packing of oxygen atoms.[20]

Based on the information from the XPS and the FTIR measurements it is clear that the deposited film contains Al in a variety of bonding environments including oxide, carbonate and hydroxide. A mild anneal of the film for 5 min in N_2 at 600°C leads to desorption of the H_2O and carbonate species and enhancement of the Al-O peaks (Fig. 2.4 curve ii). It is unclear, though, whether the C containing impurities are completely removed from the film, or more likely, if just the O species is desorbed leaving behind C in the bulk of the film.

Figure 2.5 shows the transmission IR spectrum for an Al_2O_3 film deposited from $Al(hfac)_3$ precursor with H_2O_2 as oxidizer at 130°C and 2500 psi. The spectrum shows features compatible with the presence of H_2O in the film (3600-3000 cm^{-1}) and Al-O bonding (850-500cm^{-1}). Well resolved peaks at 1700cm^{-1} and 1300-1150cm^{-1} are attributed to the presence of carbonate type and C-F bonding in the film.[21] A mild anneal for 10 min at 600°C in N_2 removes most of the IR signature of these impurities, strengthening the Al-O peaks in parallel. It is again unclear, though, whether the C and F containing impurities are completely removed from the film or more likely just the O species is desorbed leaving behind C and F in the bulk of the film.

The insulating properties of the Al_2O_3 films were evaluated by capacitance vs. voltage measurements. Figure 2.6(a) shows the high (1 MHz) and low (100KHz) frequency

C-V curve for a film that was deposited from $Al(acac)_3$ and H_2O_2 at 80°C, 2060psi, and was annealed at 600°C in N_2 for 10min. The two curves are fairly similar indicating the absence of substantial concentration of interface traps.[22] Based on the C-V data the Equivalent Oxide Thickness (EOT) of the film is 71Å, and the flatband voltage is ~ -0.14eV indicating the presence of a small amount of positive fixed charge. However, in Fig. 2.6(b) the hysteresis for the 1MHz curve for the same film is quite large (~500mV) indicating large concentrations of mobile charge in the bulk of the film.[22] This is probably due to bulk carbonate and hydroxide species detected by XPS and IR measurements. The post-deposition anneal has probably removed most of the IR signature of these species, however, it is not clear what happens to the C in the film. Previous work on LaSiO films has shown that formation of carbonates and hydroxides may recur even after high temperature anneals of the films. [23]

I.b Cyclic Deposition Method

The cyclic process was also used to deposit Al_2O_3 films from $Al(acac)_3$ precursor with either H_2O_2 or tert-butyl peracetate solutions as oxidizers. Both oxidizers were used under similar temperature and pressure conditions, at 120°C, and 1600psi. For the H_2O_2 process, for 9 cycles we measured a film thickness of ~40Å using spectroscopic ellipsometry, while for the tert-butyl peracetate based process for 12 cycles we measured a film thickness of 35Å. Thickness values from ellipsometry measurements were obtained assuming optical constants for Al_2O_3 on SiO_2. Figure 2.7 shows the high resolution XP spectra for Al 2p C1s and O1s core electrons for both films. The Al 2p spectrum (Fig. 2.7a) is substantially different for the two samples. For the film deposited with H_2O_2 (labeled HP) a peak is observed at 74.8 eV indicative of Al-O bonds. For the film deposited using tert butyl peracetate (labeled TBP) the peak is shifted to higher binding energy (~75.5eV) which

indicates bonding of the Al atoms with more electronegative species. The C 1s spectrum shows the existence of adventitious C (peak at 285 eV) for both samples. For sample HP a second peak at 289.3eV is well resolved evidence of carbonate formation in the film. For sample TBP the C1s spectrum tails toward the higher binding energies with a shoulder at ~289.5 eV. The O1s spectra for both samples are quite similar containing contributions from SiO_2, Al_2O_3 and various hydroxides and carbonates.

From the relative intensity of the Al 2p peak (note the 10x multiplication factor for the tert-butyl peracetate sample) we can conclude that the Al content of the TBP film is significantly lower than for the HP and/or the TBP film is much thinner. Based on the binding energies of the O 1s electrons in Al_2O_3 (74.6eV), AlO(OH) (76.7eV) and $Al(OH)_3$(74.3-75.9eV) we can conclude that the two films show evidence for hydroxides and carbonates. However, the proportion of these components in each film appears to be quite different. From the location of the Al2p peak we conclude that a) film TBP has a small Al_2O_3 content and most of the Al is bonded as AlO(OH) and b) film HP has a higher Al_2O_3 and $Al(OH)_3$ content and some carbonate content. The carbon content is difficult to analyze by ex-situ XPS due to the adventitious carbon from the environment. The higher OH content for film HP can be justified from the use of the aqueous H_2O_2 solution during the oxidation reaction. The process cycle for TBP film does not include exposure to H_2O, however, Al oxides are hydrophilic and most likely the film absorbed H_2O from the ambient after removal from the high pressure cell. It is not clear whether the carbonate formation occurs during the reaction or after ambient exposure. Other group III based oxides and silicates are very susceptible to reactions with atmospheric carbon dioxide to form various types of carbonate species.[23]

II. Batch Deposition of other Metal-Oxide Films

In addition to Al_2O_3 several other metal organic precursors were tested in similar conditions. Table 2.1 gives a summary of all films deposited, including the precursor used, and the oxidizing agent. Also included in the table are observations of general solubility of the precursors, and whether film formation was observed. The following section contains XPS characterization data for some of these films.

II.a Zr based films

Figure 2.8 shows the Zr 3d, C1s, and O1s portions of the XP spectra for a Zr-based film that was deposited via CFD at 150°C, and 1700psi using $Zr(acac)_4$ and tert-butyl peracetate as reagents. The Zr 3d peaks (Fig. 2.8a) are clearly resolved at binding energies of 183 for the $3d_{5/2}$ and 185.3 eV for the $3d_{3/2}$ which is in good agreement generally accepted binding energies for ZrO_2.[24]The two peaks are separated by 2.5eV, in good agreement with the 2.4eV splitting reported.[24] The width of the peaks however suggests the presence of additional binding environments for the Zr atoms. For example, the binding energy of the Zr $3d_{5/2}$ electrons in the Zr-OH state is reported to be at 183.4 ~0.5 eV higher than that in ZrO_2 [25] The width of the O1s peak (Fig. 2.8c), located at ~532.5 eV, corroborates the conclusion. The binding energy for the O1s electrons in the Zr-OH state has been measured at 531.5 eV and that of Zr bound to H_2O at 533.3 eV.[18], [26]. Additionally, 1s electrons emanating from O in carbonate bonding have a binding energy of 532 eV. The C1s high resolution spectrum exhibits a peak at 589.5eV, consistent with carbonate presence in the film. Based on the above observations we can conclude that the Zr-based film contains a mixture of ZrO_2, Zr-OH and Zr-carbonate.

II.b Ru based films

Figure 2.9 shows the survey spectrum for a Ru based film deposited from $Ru(tmhd)_3$ and H_2O_2 at 150°C, 3600 psi. The Ru 3p and Ru 3d peaks are clearly visible, along with the O1s, C1s and Si 2p peaks. High resolution spectra of the Ru 3d region at 270-295 eV and the O1s region at 525-535 eV is shown on Fig. 2.10a and 2.10b respectively. The Ru 3d peaks overlap partially with the C1s peak, but the lowest binding energy for a carbon peak is that of adventitious carbon at 285. Based on that, the peak at ~281.1 eV is assigned to the $3d_{5/2}$ component. The existence of the Ru 3p peaks in the survey spectrum corroborates the presence of Ru in the film and the previous peak assignment. Ru can form several oxides that vary in the binding energy of the Ru 3d peaks. For RuO_2 the $3d_{5/2}$ electrons appear at 280.6eV [27] while the ones from RuO_3 at 282.5eV [28]. The location of the observed peak at 281.1eV may indicate the existence of both RuO_2 and RuO_3 in the film. On the O1s spectrum presented on Fig. 10b the locations are marked for the O1s electron signals from RuO_2 (529.4eV [28]) and RuO_3 (530.7eV [27]). The peak in Figure 2.10(b) is fairly broad and confirms that both oxidation states are present in the film. However, based on the O1s data we can not exclude the presence of Ru-OH or Ru carbonate species either.

RuO_x deposition was also achieved by using Bis (cyclopentadienyl) ruthenium (ruthenocene) and H_2O_2 at 130°C and 3120 psi. Figure 2.11 shows the survey spectrum that includes the Ru 3p, Ru 3d O1s, C1s and Si 2p peaks. Figure 2.12 shows the O1s, Ru3d/C1s regions in high resolution. The conclusions regarding the composition of the film are pretty similar to the previous Ru-based film deposited from $Ru(tmhd)_3$ and H_2O_2.

II.c Mn based films

Finally Figure 2.13 presents the survey spectrum for a Mn based film, deposited from $Mn(hfac)_3$ and H_2O_2 at 150°C and 3500psi. There are several peaks in the survey spectrum; the most intense are the Mn2p, O1s, C1s, F1s and Si2p. High resolution spectrum for C1s, O1s and Mn2p are shown on Fig 2.14(a),(b), and (c) respectively. For the Mn 2p peaks the $2p_{3/2}$ and $2p_{5/2}$ are located at 653.9 eV and 642 eV and show a splitting of 11.9 eV in good agreement with the 11.7 eV generally cited. [29] Mn appears in oxides with a variety of oxidation numbers and the 2p core electrons reflect that difference in the binding energy. For the $2p_{5/2}$ component binding energies range from 640.5 eV for MnO [30] to 642.2 eV for MnO_2 [31]. Other Mn-based oxides are Mn2O3 with a binding energy of 642 eV [29] and Mn_3O_4 with a binding energy of 641.2 [30]. Finally, Mn bound in MnO(OH) has a binding energy of 641.7 eV. [30] On Fig. 2.14 c we shade the extended region where these peaks occupy and classify all the oxides as MnO_x. Most likely the film contains most or all of these oxides and hydroxides. Also, since the Mn peaks occupy a more extended region than the MnO_x highlighted area we can conclude that Mn must be bound to O in other configurations and/or bound to other elements. The C1s and O1s peaks offer nore clues in that direction. On the C1s plot (Fig. 2.14a) we see a peak at 288.8 eV indicative of carbonate bonding. The O1s peak (Fig. 2.14 b) is located at 531.7 eV and covers a broad range. All the MnO_x-Mn(OH)O compounds have O1s binding energies inside the highlighted area. From the peak location we conclude that although oxide is present in the film, most likely the dominant bonding environment is that of carbonate and hydroxide with binding energies at 532eV [17] and 532.8 eV [32].

2.4 DISCUSSION

Several metal oxides films have been deposited using precursors soluble in supercritical carbon dioxide. Use of the aqueous H_2O_2 solutions as oxidizer generally leads to hydroxide and carbonate concentration. It is well established that exposure of metal oxide powders to carbon dioxide in an environment with high moisture concentration promotes the formation of carbonate species.[33],[34] We conclude that H_2O in the cell during the reaction is likely responsible for the large extent of carbonate formation.

For the batch process the aqueous solution of H_2O_2 is the most successful oxidizing agent for film growth. Both H_2O_2 and H_2O have low solubility in sc CO_2 and thus are not considered very desirable oxidizers for this process. It is possible that the solvation energy, along with the mild thermal energy provided in the reaction, is sufficient to liberate reactive atomic oxygen from the peroxide. A serious drawback of using the hydrogen peroxide solution is absorption of water into the metal oxide film as confirmed by infrared and XPS measurements. A non aqueous oxidizer is highly desirable especially for applications involving the hygroscopic group III metal oxides. A non-aqueous highly soluble tert-butyl peracetate solution was tested, which has been used successfully in the removal of Cu(0) during a sc CO_2 based "dry" chemical mechanical planarization process[35]. Thin film growth was observed using this oxidizer, but growth rates were generally low. This is attributed to homogeneous reactions between the dissolved metal precursor and the oxidizer.

To prevent reactions of the precursor with the oxidizer in the supercritical phase the two reagents were introduced in the cell sequentially, mimicking an ALD process. In that scheme, since the two reagents do not coexist in the cell only surface reactions are feasible. Using this cyclic approach, deposition of films was demonstrated using both H_2O_2 and tert-

butyl peracetate solutions as oxidizers. SE measurements analyzed using the optical constants of Al_2O_3 and SiO_2, indicated that the deposition rate for the process using the organic peroxide is lower but comparable to that of H_2O_2. However, comparison of the XPS Al 2p peak intensities suggests that the film TBP deposited with tert-butyl peracetate solutions has a substantially lower Al content. IR and XPS measurements confirm the presence of Al atoms bound in carbonate and hydroxide configurations. Based on that it appears that the extraction of film thickness based on the two layer model maybe not be suitable for such films. The optical constants of the deposited Al films depend on the specific carbonate and hydroxide film content and may deviate substantially from the optical constant of Al_2O_3. Since the film from tert-butyl peracetate has a lower Al_2O_3 content than films from peroxide, the uncertainty in thickness obtained from the ellipsometry measurement is substantially higher. For the films from hydrogen peroxide, the deposition rate as calculated from ellipsometry is larger than one monolayer per cycle, where as typical deposition rates for self-limiting vacuum based ALD are of sub-monolayer per cycle. In our high pressure reactor, exposure of the substrate to the precursor likely leads to the deposition of several monolayers of precursor that remain on the surface during chamber purging. When the oxidizer is introduced into the cell, reaction with the precursor multilayer results in film growth of 2-3 monolayers per cycle.[36]

2.5 CONCLUSIONS

We have demonstrated deposition of Al, Zr, Ru and Mn based thin oxide films using supercritical carbon dioxide as a means for metal organic precursor dissolution and delivery. Hydrogen peroxide aqueous solution and tert butyl peracetate solutions were tested as oxidizing agents. Although H_2O_2 has very poor solubility in sc CO_2 it proved a more successful oxidizer for Al_2O_3 thin film deposition in a batch process. For a similar Al_2O_3

cyclic deposition process, both oxidizers resulted in film formation. Carbon and H_2O contamination in the films was detected via IR and XPS measurements. Evaluation of the electrical properties of Al_2O_3 films revealed the formation of a good quality interface but the presence of large concentrations of mobile charge in the films. Further refinement of the experimental technique with the development of a process that does not include H_2O is expected to address some of these issues. However, the initial results presented in this article indicate that a supercritical fluid based thin film deposition technique may provide a viable alternative to vacuum based processes.

2.6 ACKNOWLEDGEMENS

Financial support from NSF (Grant# CTS-0304296) and the NSF Science and Technology Center for Environmentally Responsible Solvents and Processes is gratefully acknowledged. We would also like to acknowledge Ke Wang for assistance with the sc CO_2 experimental set up and Ruben Carbonell for helpful discussions.

2.7 REFERENCES

1 N. Petrov, Y. Sverdlov, and Y. Shacham-Diamond, Journal of the Electrochemical Society **149,** C187 (2002)

2 *Electroless Plating - Fundamentals and Applications*; *Vol.*, edited by G. O. Mallory and J. B. Haydu (American Electroplaters and Surface Finishers Society, Orlando, 1990)

3 M. McHugh and K. V, *Supercritical Fluid Extraction* (Butterworth-Heinemann, Boston, 1994)

4 J. M. DeSimone, E. E. Maury, Y. Z. Menceloglu, J. B. McCain, T. J. Romack, and J. R. Combes, Science 265, 356 (1994).

5 J. M. Blackburn, D. P. Long, A. cabanas, and J. J. Watkins, Science 294, 141 (2001)

6 D.P Long, J. M. Blackburn, and J. J. Watkins, Advanced Materials 12, 913 (2000)

7 J. J. Watkins, J. M. Blackburn, and T. J. McCarthy, Chem. Mat.s 11, 213 (1999).

8 J. W. Rathke, R. J. Klinger, and T. R. Krause, Organometallics **10,** 1350 (1991)

9 G. D. Wilk, R. M. Wallace, and J. M. Anthony, J. Appl. Phys. **89** (10), 5243 (2000).

10 J. M. DeTeresa, A. Barthelemy, A. Fert, J. P. Contour, F. Montaigne, and P. Seneor, Science **286**, 507 (1999).

11 K. Domen, T.J. Chuang, J. Chem. Phys. **90**, 3318 (1989).

12 K. Arata, M. Hino, Appl. Catalysis **59**, 197 (1990)

13 J.R. Lindsay, H.J. Rose, W.E. Swartz, P.H. Watts, K.A. Rayburn, Appl. Spectrosc. **27**, 1 (1973).

14 J.A. Taylor J. Vac. Sci. Technol. **20**, 751 (1982)

15 E. Paparazzo Appl. Surf. Sci. **25**, 1 (1986).

16 C.D. Wagner, D.E. Passoja, H.F. Hillery, T.G. Kinisky, H.A. Six, W.T. Jansen, J.A. Taylor, J. Vac. Sci. Technol. **21**, 933 (1982).

17 G. Bandoli, D. Barreca, E. Brescacin, G. A. Rizzi and E. Tondello, Adv. Mater. : Chem. Vap. Dep. **2**, 238 (1996).

18 J. F. Moulder, W. F. Stickle, P. W. Sobol and K. D. Bomben, Handbook of X-ray Photoelectron Spectroscopy, Perkin-Elmer, Physical Electronics Division, Eden Prairie, MN, 1992.

19 G. Cerrato, S. Bondiga, S. Barbera, and C. Morterra, Appl. Surf. Sci. 115, 53 (1997).

20 P. Madhu Kumar, C. Balasubramanian, N. D. Sali, S.V. Bhoraskar, V.K. Rohatgi, and S. Badrinarayanan, Mater. Sci. Eng. B **63**, 215 (1999).

21 K. K. S. Lau, J. A. Caulfield, and K.K. Gleason, Chem. Mater., 12, 3032 (2000)

22 D. K. Schroder, Semiconductor Material and Device Characterization, Second Edition, Wiley Interscience, New-York NY, p.338 (1998)

23 T. Gougousi, and G.N. Parsons, J. Appl. Phys. **95**(3), 1391 (2004),.

24 S. Sinha, S. Badrinarayanan, A.P.B. Sinha ,J. Less-common Metals **125**, 85 (1986).

25 Y. S. Li, P. C. Wang, and K. A. R. Mitchell, Appl. Surf. Sci. **89** (1995)

26 B. Basu, R. G. Vitchev, J. Vleugels, J. P. Celis and O. Van Der Biest, Key Eng. Mater. **206-213**, 783 (2002)

27 D.D. Sarma, and C.N.R. Rao, J. Electron Spectrosc. Relat. Phenom. **20**, 25 (1980)

28 K.S. Kim, and N. Winograd, J. Catal. **35**, 66 (1974)

29 B.J. Tan, K.J. Klabunde, and P.M.A. Sherwood, J. Am. Chem. Soc. **113**, 855 (1991)

30 M. Oku, and K. J. Hirokawa, Electron Spectrosc. Relat. Phenom. **8**, 475 (1976).

31 G.C. Allen, S.J. Harris, J.A. Jutson, and J.M. Dyke, Appl. Surf. Sci. **37**, 111 (1989).

32 N. Martensson, P.A. Malmquist, S. Svensson, E. Basilier, J.J. Pireaux, U. Gelius, and K. Siegbahn, Nouveau J. Chim. **1**, 191 (1977).

33 C. Morterra, G. Cerrato, S. Di Ciero, Appl. Surf. Sci. 126 107 (1998)

34 S. Takeda, M. Fukawa, Y. Hayashi, K. Matsumoto, Thin Solid Films 339, 220 (1999)

35 C. A. Bessel, G. M. Denison, H. M. DeSimone, J. DeYoung, S. Gross, C. K. Schauer, and P. M. Visintin, J. Am. Chem. Soc. **125**, 4980 (2003).

36 D. Barua, T. Gougousi, E. D. Young and G. N. Parsons in preparation.

Table 2.1

Material	Precursors	solubility	oxidizer	Method	Temperatures Studied (°C)	Comments
Al2O3	Al acac	poor	30% H2O2 in H2O	batch	70 - 120	thick films
			50% tert butyl peracetate in mineral spirits	batch	120	thinner films, precipitates
			oxygen	batch	120	no visible film
	Al acac	poor	30% H2O2 in H2O	cyclic	120	multilayer growth per cycle
			50% tert butyl peracetate in mineral spirits	cyclic	120	thinner growth per cycle
	Al hfac	very good	30% H2O2 in H2O	batch	80 - 120	thick films, with fluorine
			50% tert butyl peracetate in mineral spirits	batch	150	thin films, with Fluorine
ZrO2	Zr acac	poor	30% H2O2 in H2O	batch	120 - 200	thin film
			50% tert butyl peracetate in mineral spirits	batch	150	thin film
HfO2	Hf acac	poor	30% H2O2 in H2O	batch	120 - 200	not characterized
	TDEAHf	precursor oxidized	30% H2O2 in H2O	batch	100 - 150	precipitates
ZnOx	Zn(hfac)	very good	30% H2O2 in H2O	batch	150	not characterized
MnOx	Mn hfac	very good	30% H2O2 in H2O	batch	100 - 150	thin film
RuOx	Ru tmhd	good	30% H2O2 in H2O	batch	100 - 150	thin film
			50% tert butyl peracetate in mineral spirits	batch	100 - 120	thin film
	Ru Cp2	poor	30% H2O2 in H2O	batch	90 - 180	thin film
Y2O3	Y tmhd	good	30% H2O2 in H2O	batch	120 - 150	thick film, carbon contamination

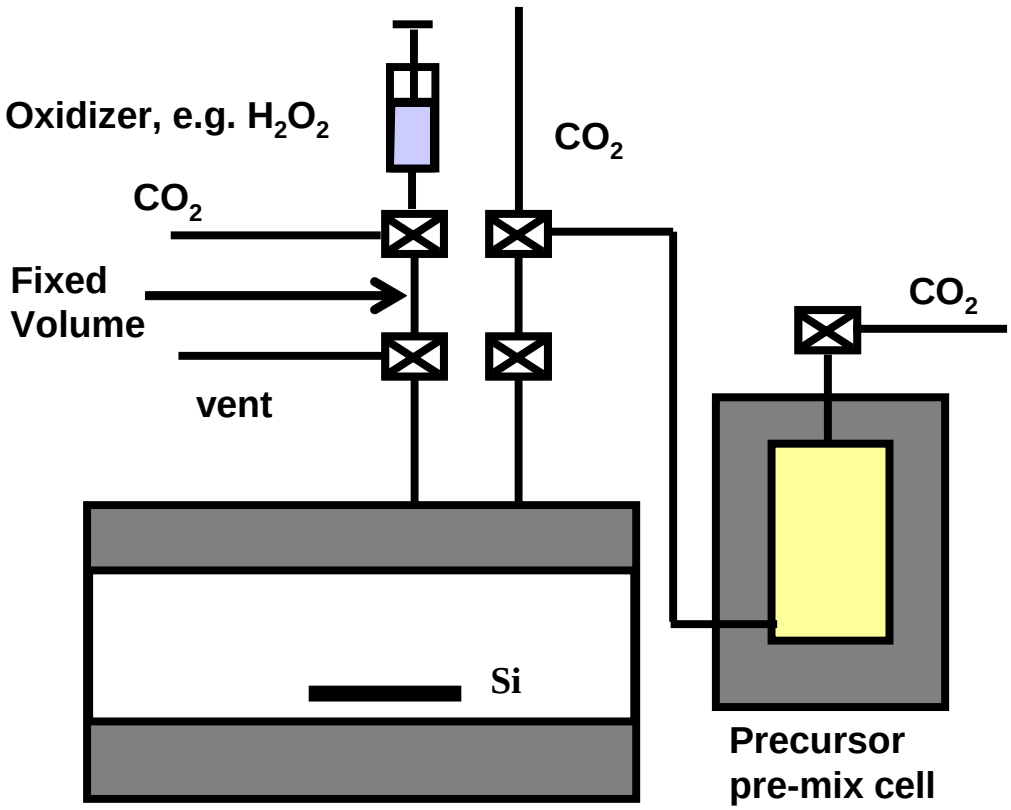

Figure 2.1 A schematic of the deposition system

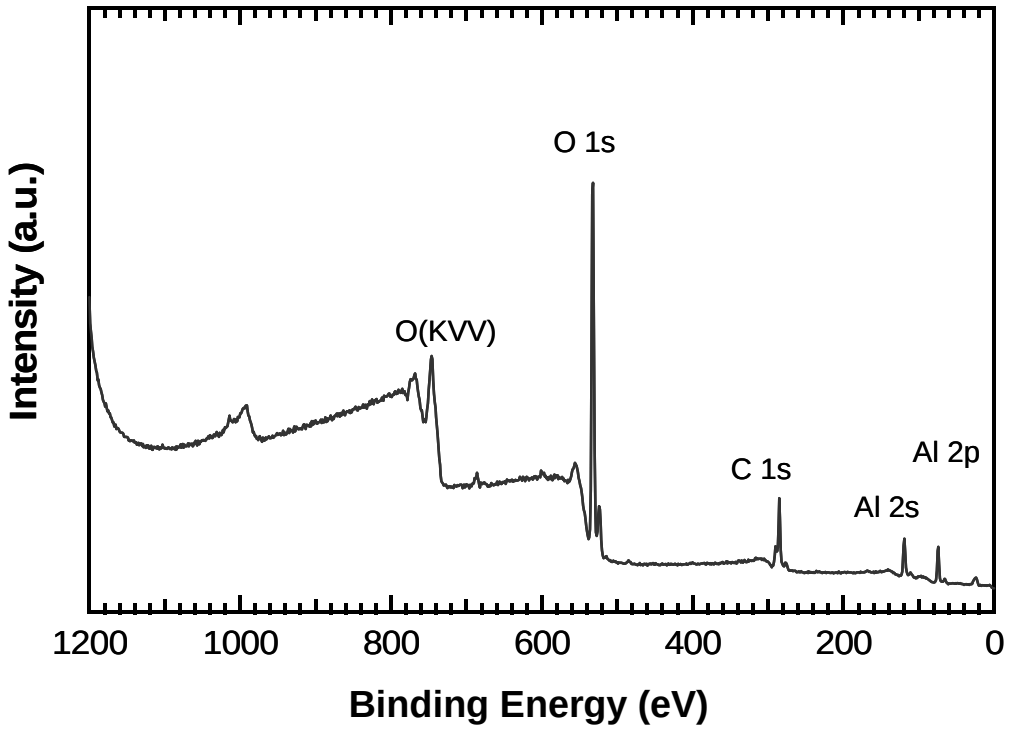

Figure2.2 XPS survey scan for an Al based film deposited from $Al(acac)_3$ and H_2O_2 at at 120°C and 1700 psi . Peaks assigned to Al 2s, Al 2p , C1s and O1s core electrons can be distinguished.

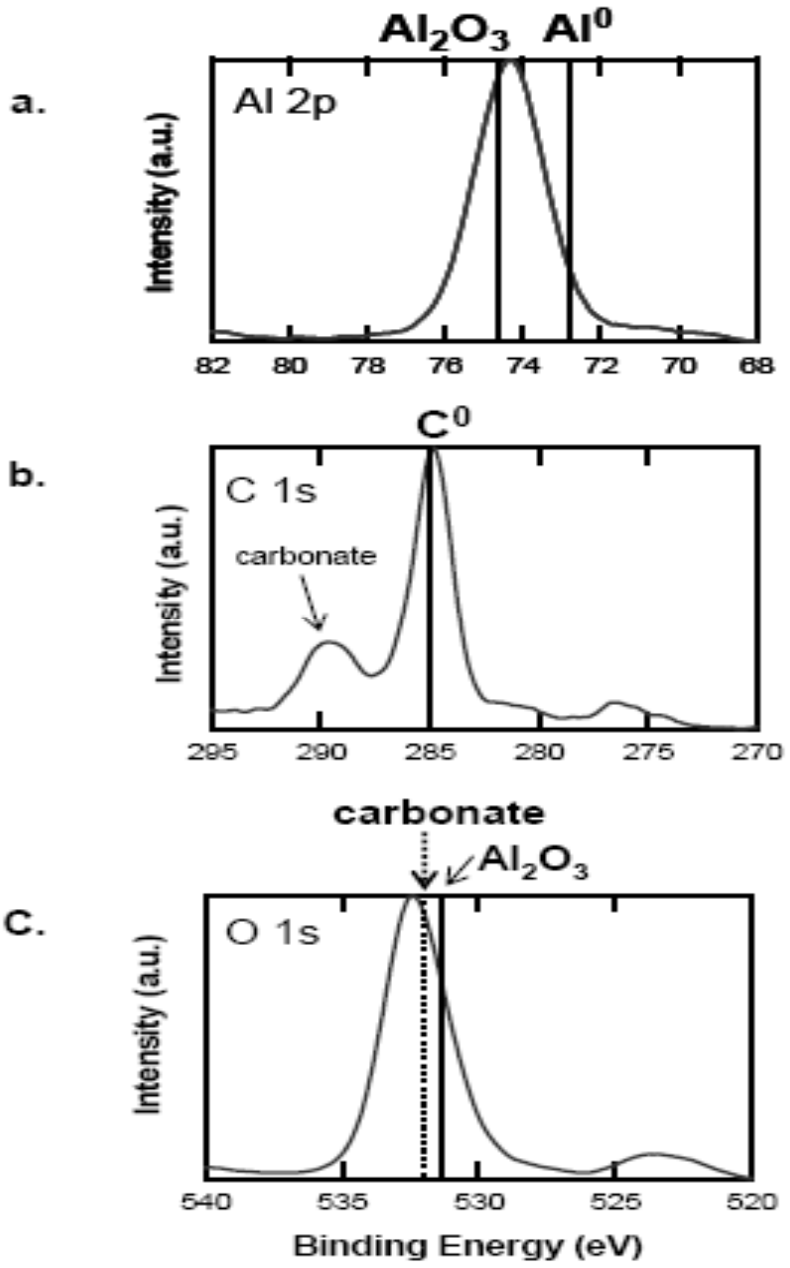

Figure 2.3 High resolution scans for the (a) Al 2p, (b) C1s and (c) O1s peaks for XPS survey scan for an Al based film deposited from $Al(acac)_3$ and H_2O_2 at 120°C and 1700 psi on Si substrates with native oxide. From the location and width of the peaks we conclude that the film is a mixture of Al_2O_3, Al(OH)O and Al-carbonate.

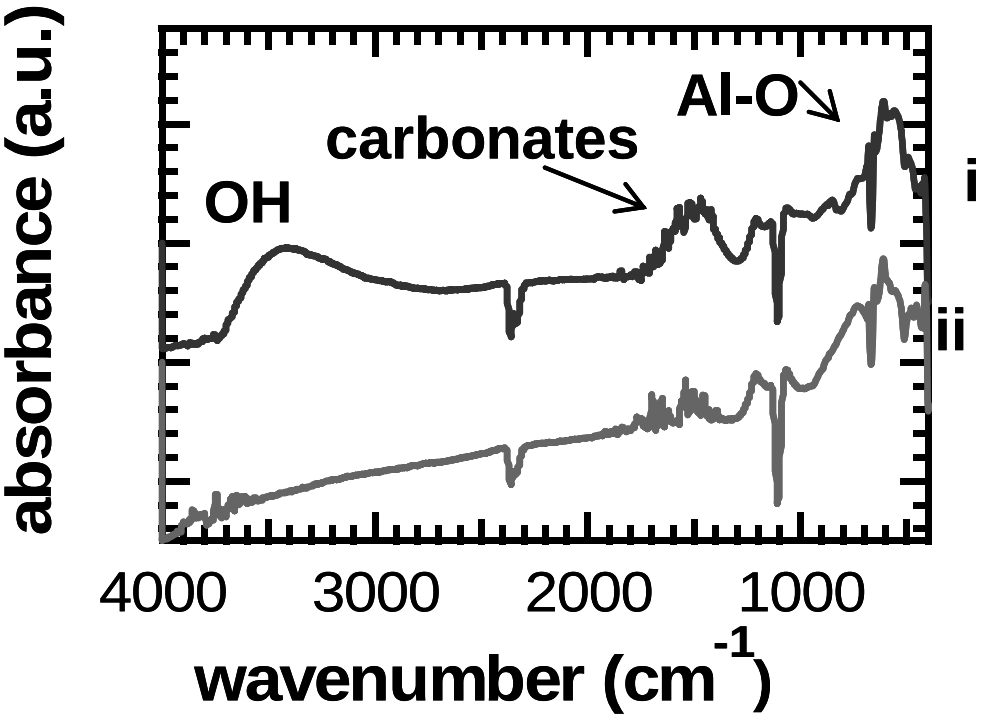

Figure 2.4 Transmission IR spectrum for an Al-based film deposited from $Al(acac)_3$ and H_2O_2 at 120°C and 1700 psi on Si substrates with native oxide. Curve (i) shows a measurement taken after film deposition and curve (ii) shows a spectrum taken after the film was annealed at 600°C in N_2 for 5 min. Spectrum (i) exhibits features at 1200-1700 cm^{-1} associated with several carbonate species. The broad peak at 3000-3600 cm^{-1} is due to the O-H stretching modes of both undissociated H_2O molecules and surface H-bonded OH species. Al-O bonding is detected by the borad peak at 400-800cm^{-1}. Mild anneal result in the disappearance of the IR signature of the carbonates and hydroxides.

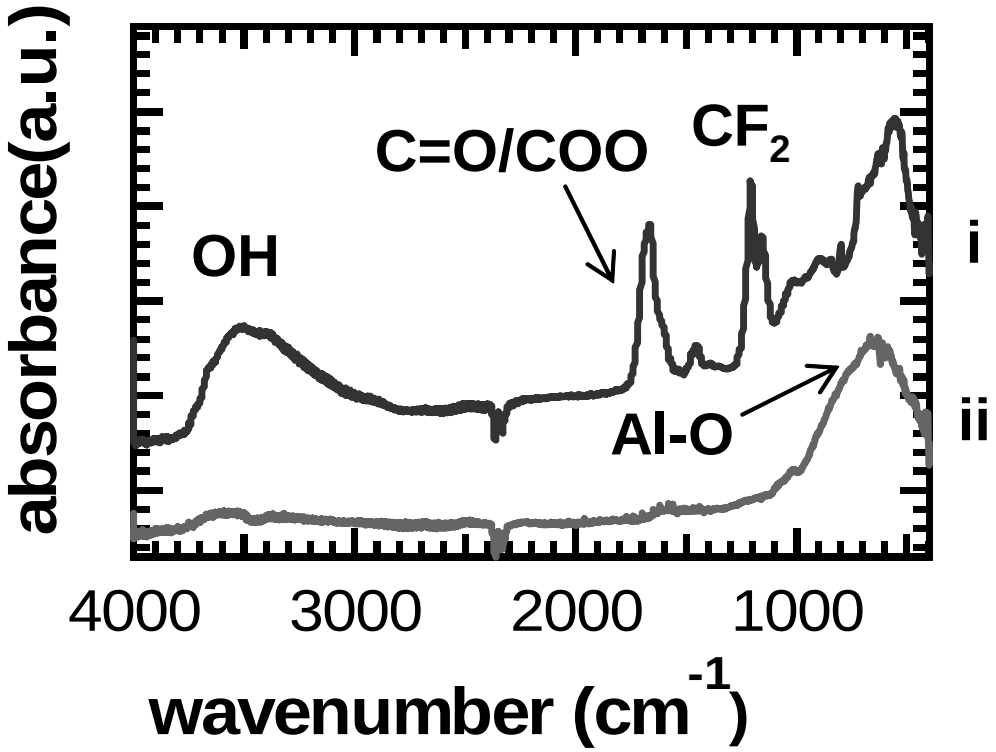

Figure 2.5 Transmission IR spectrum for an Al-based film deposited from $Al(hfac)_3$ and H_2O_2 at 130°C and 2500 psi. The spectrum shows features compatible with the presence of H_2O in the film (3600-3000 cm^{-1}) and Al-O bonding (850-500cm^{-1}). Well resolved peaks at 1700cm^{-1} and 1300-1150cm^{-1} are attributed to the presence of carbonate type and C-F bonding in the film. A mild anneal for 10 min at 600°C in N_2 removes most of the IR signature of these impurities, and reinforces the Al-O peak.

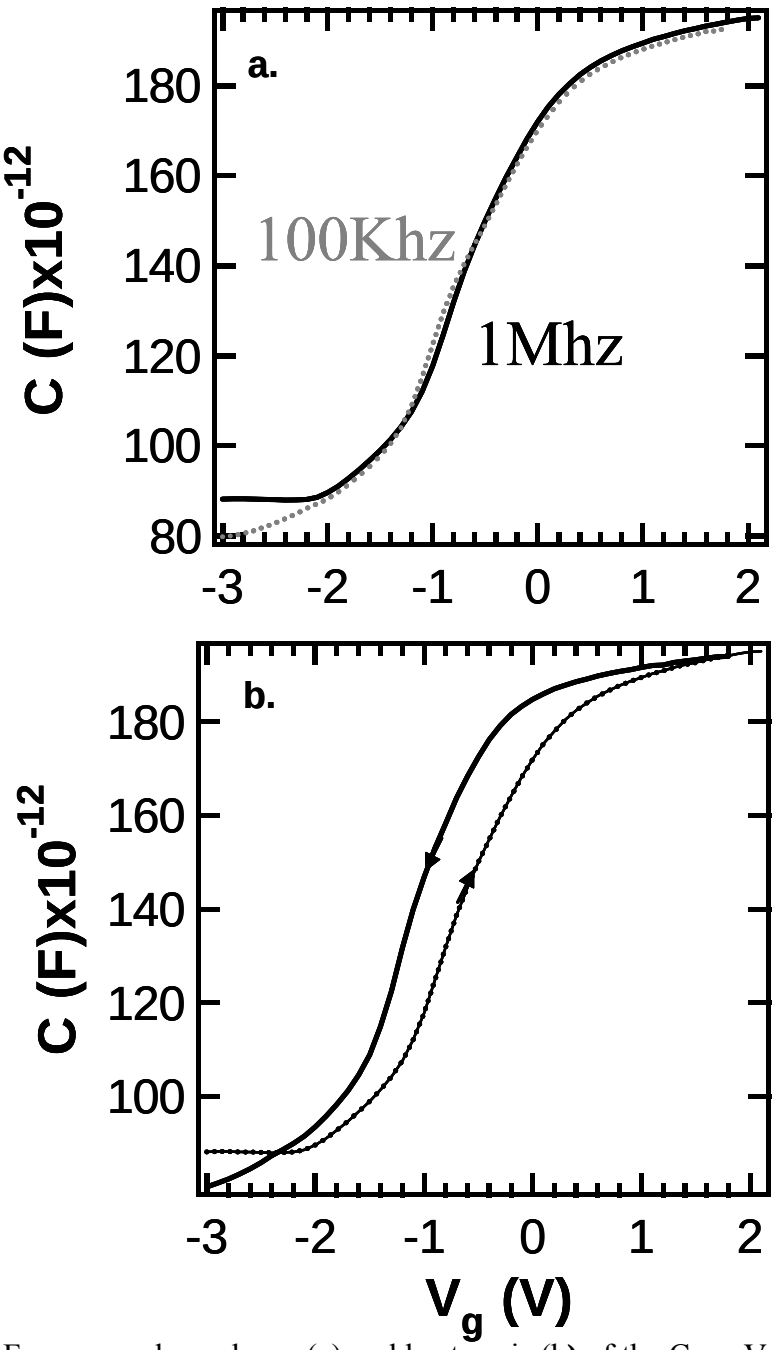

Figure 2.6 Frequency dependence (a) and hysteresis (b**)** of the C vs. V measurements for Al-based film deposited from $Al(acac)_3$ and H_2O_2 at 80°C , 2060 psi and annealed at 600°C in N_2 for 10 min. Change of frequency from 1MHz to 100 KHz does not change the shape of the curve substantially indicating good quality interface. However, the hysteresis is quite large ~500 mV.

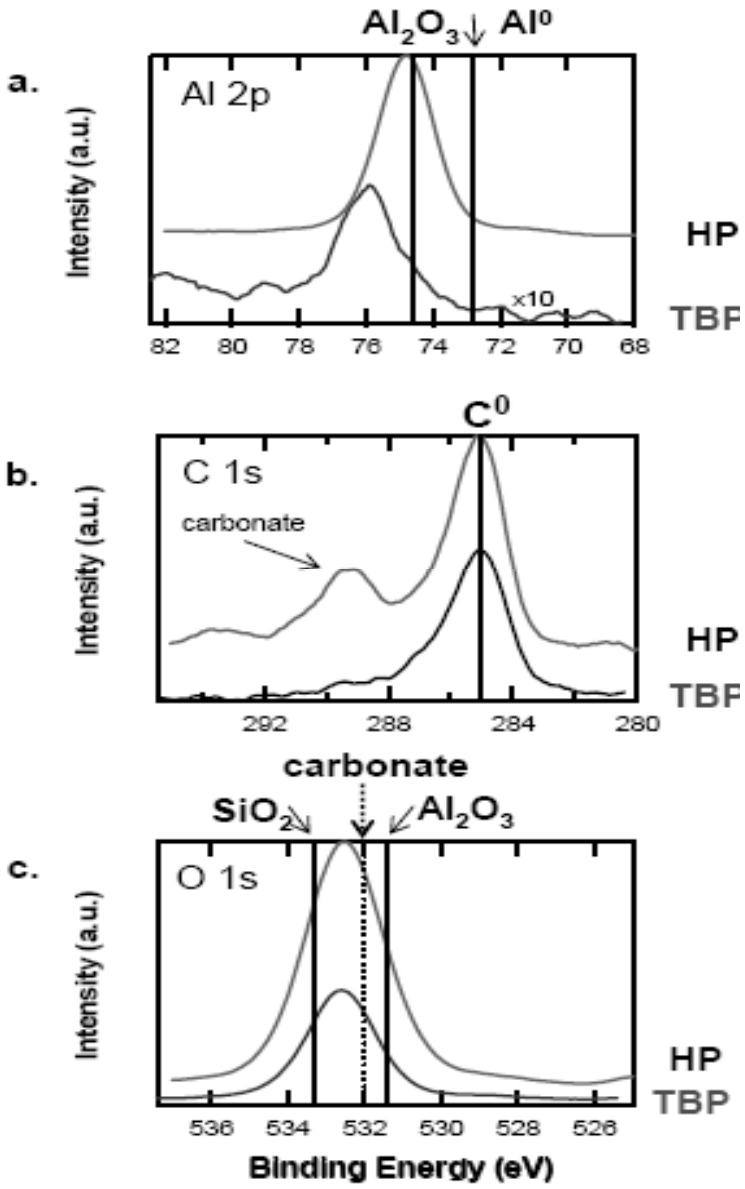

Figure 2.7 High resolution XP scans for the (a) Al 2p, (b) C1s, and (c) O1s peaks for two aluminum based films deposited via reagent cycling. Both films were deposited at 120°C, and 1600 psi. Film marked HP was deposited form $Al(acac)_3$ and H_2O_2, while film TBP was deposited from $Al(acac)_3$ and tert-butyl peracetate.

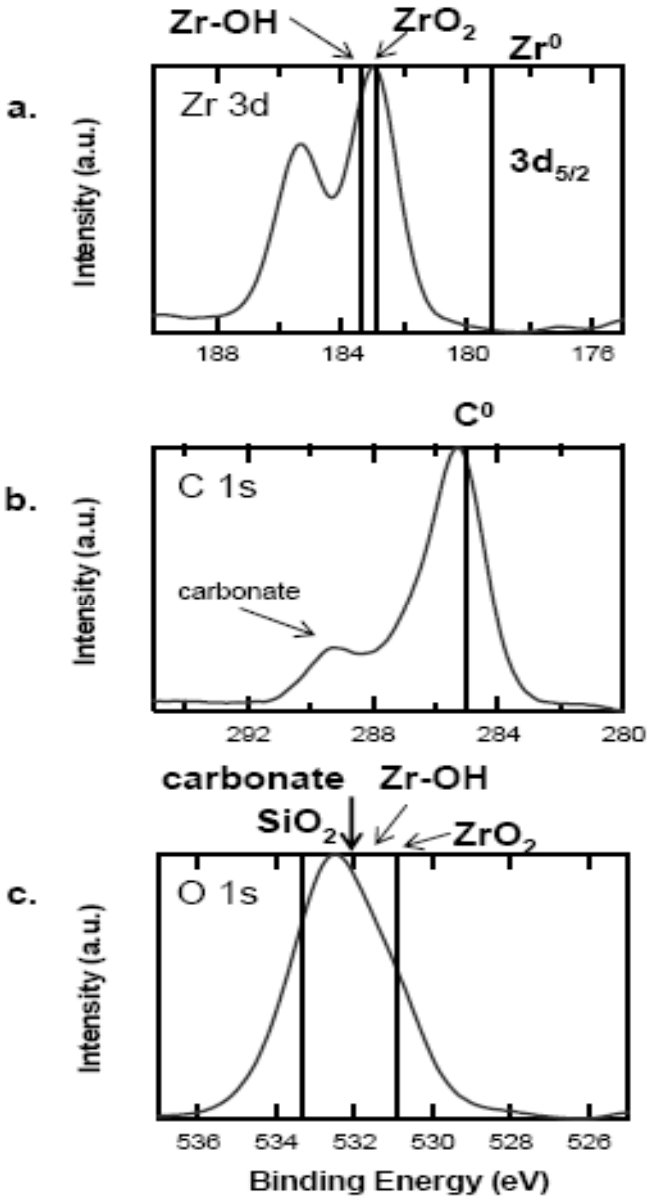

Figure 2.8 High resolution XP scans for the (a) Zr 3d, (b) C1s, and (c) O1s peaks for a Zr based film deposited from $Zr(acac)_4$ and tert-butyl peracetate at 150°C, and 1700psi. The film composition can best be described a hydroxycarbonate.

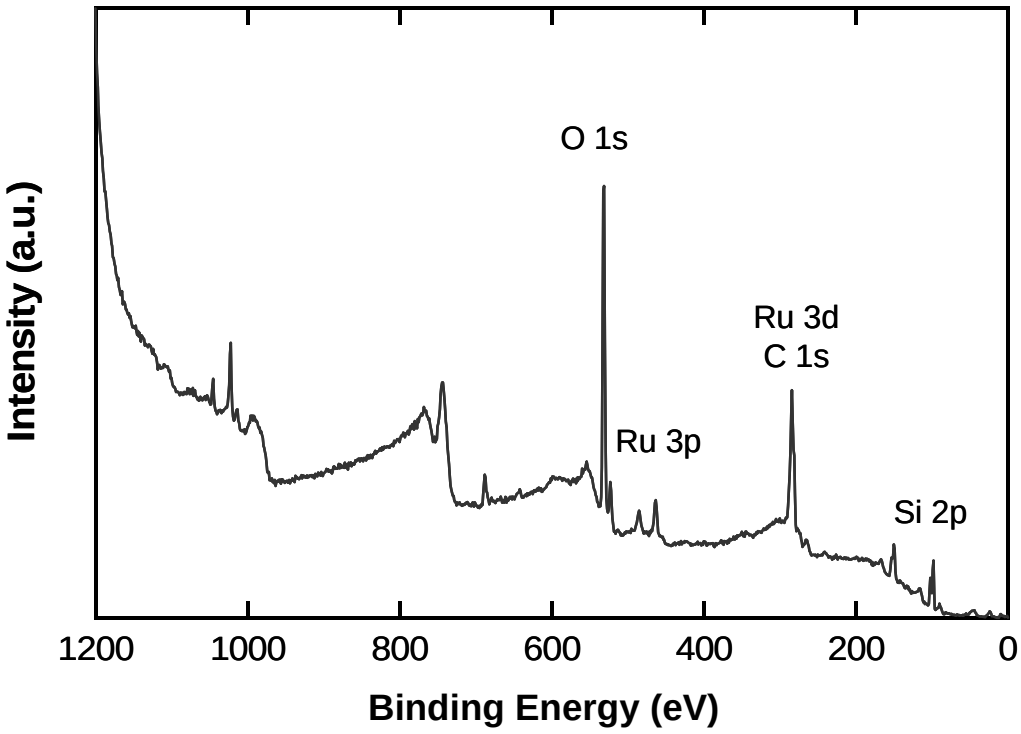

Figure 2.9 XP survey spectrum for a Ru based film deposited from $Ru(tmhd)_3$ and H_2O_2 at 150°C, 3600 psi. The presence of the Ru 3d and Ru 3p peaks verify the deposition of a Ru-based film on Si substrate.

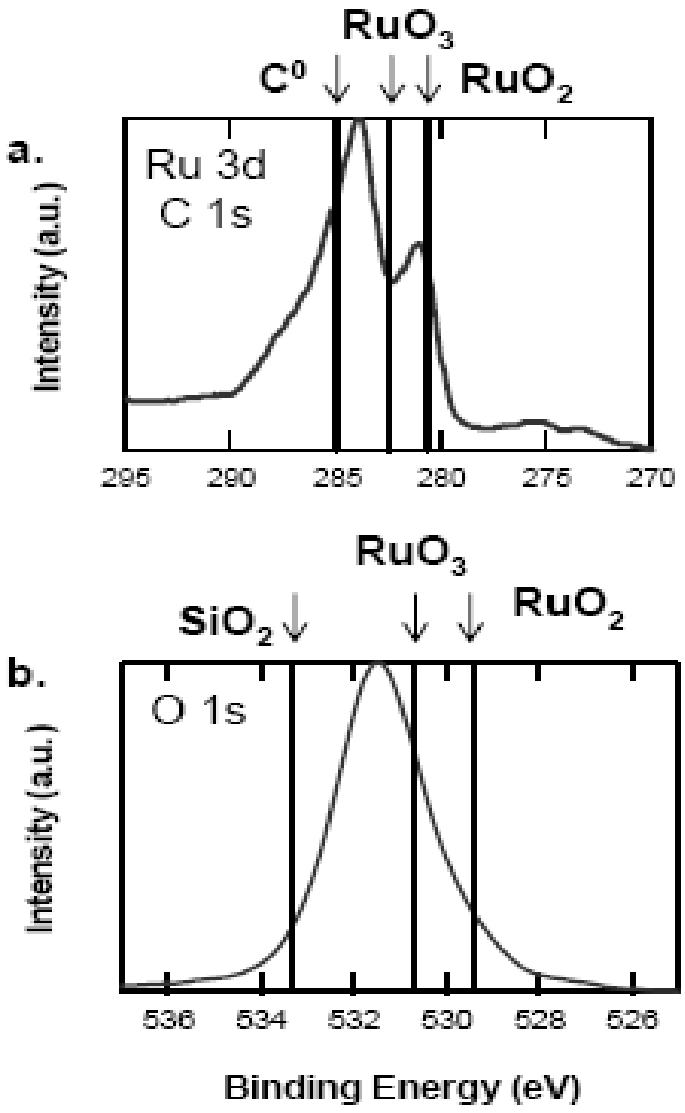

Figure 2.10 High resolution XP scans for the (a) Ru 3d- C1s, and (b) O1s peaks for a Ru based film deposited from $Ru(tmhd)_3$ and H_2O_2 at 150°C, 3600 psi. The film contains a mixture of Ru oxides and possibly carbonates and hydroxides.

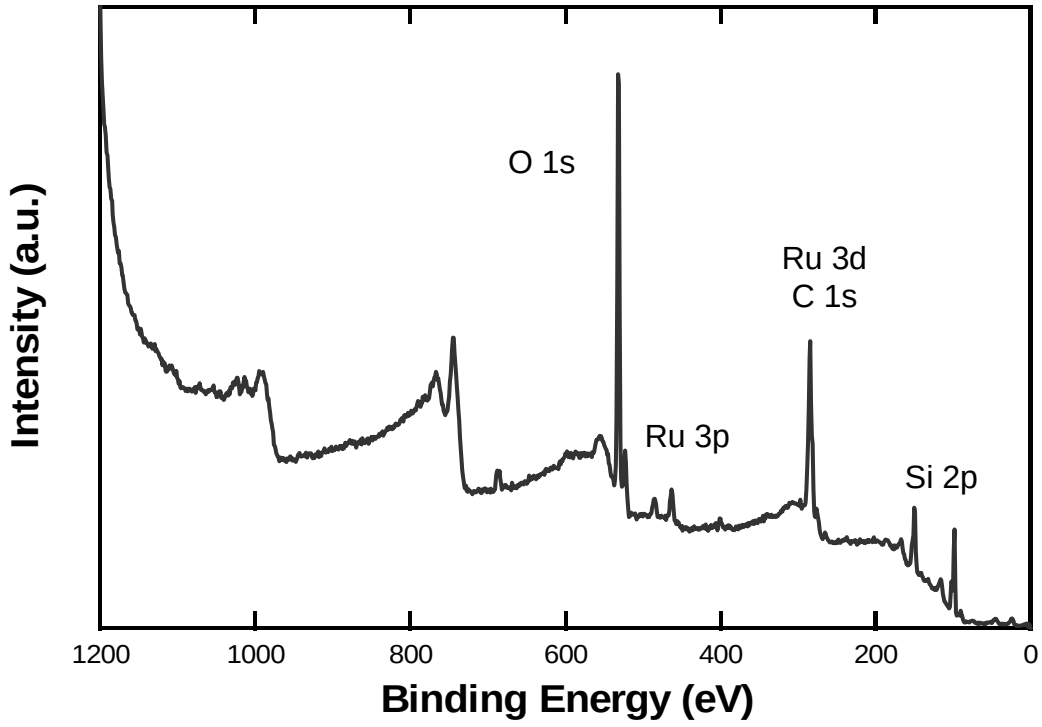

Figure2.11 XP survey spectrum for a Ru based film deposited from ruthenocene and H_2O_2 at 130°C, 3120 psi. The presence of the Ru 3d and Ru 3p peaks verify the deposition of a Ru-based film on Si substrate.

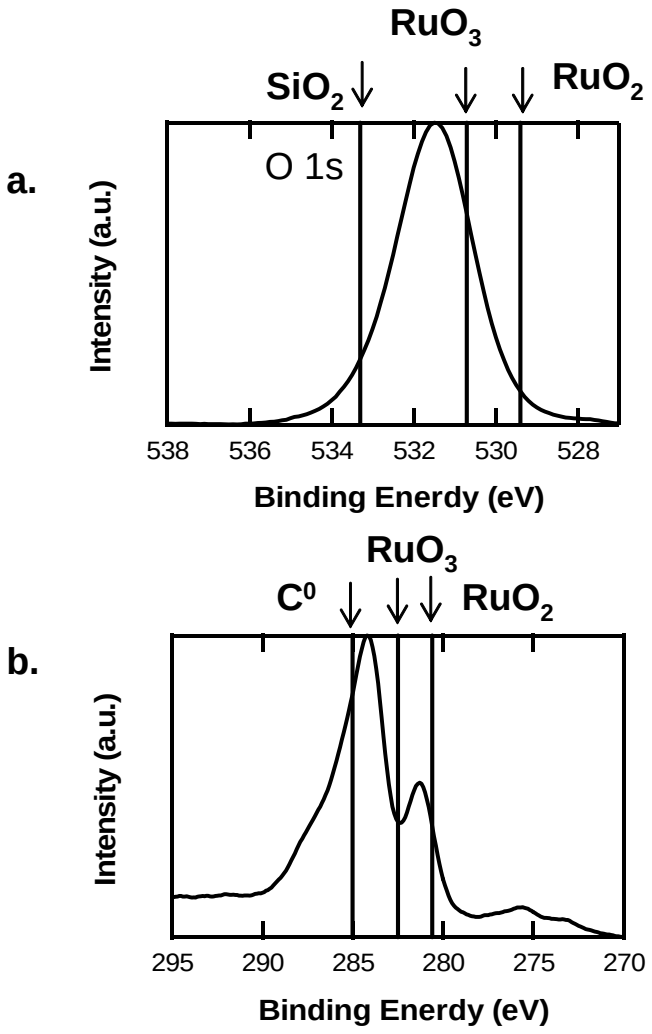

Figure2.12 High resolution XP scans for the (a) Ru 3d- C1s, and (b) O1s peaks for a Ru based film deposited from ruthenocene and H_2O_2 at 130°C, and 3120 psi. The film contains a mixture of Ru oxides and possibly carbonates and hydroxides.

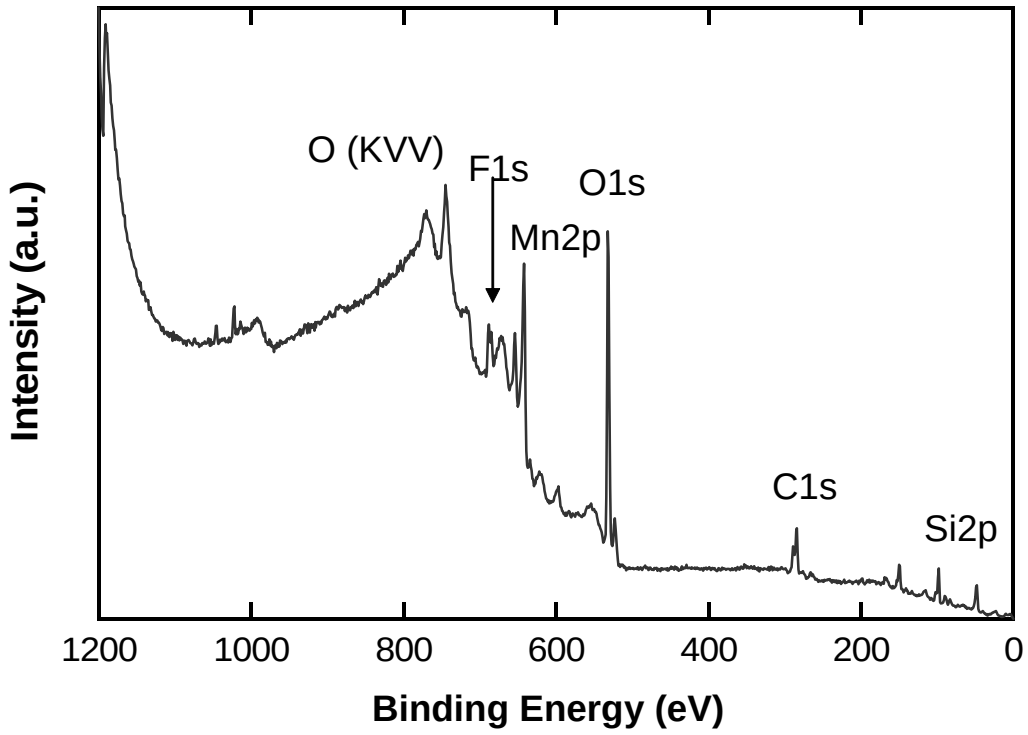

Figure2.13 XP survey spectrum for a Mn based film deposited from $Mn(hfac)_3$ and H_2O_2 at 150°C and 3500 psi. Fluorine from the precursor is observed in the film.

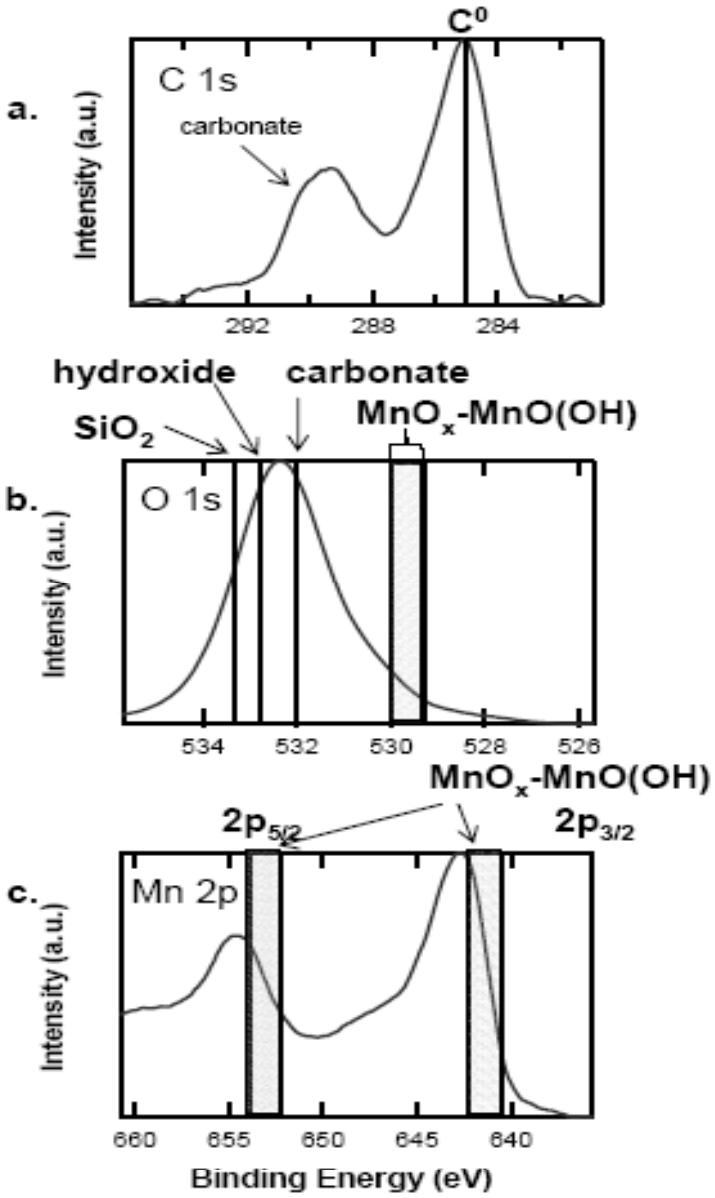

Figure2.14 High resolution XP scans for the (a) C1s, (b) O1s and (c) Mn 2p peaks for a Mn based film deposited from $Mn(hfac)_3$ and H_2O_2 at 150°C and 3500 psi. The highlighted area on plots b and c show the range of binding energies available to O 1s and M2p electrons due to the large number of oxidation states available to the Mn atoms. The film contains a mixture of Mn oxides with carbonates and hydroxides.

CHAPTER THREE

3 Cyclic/Atomic Layer depositions of Metal-Oxide and Metal Thin Films from Metal Organic Precursors in Supercritical CO_2 Solution

3.1 INTRODUCTION

Supercritical carbon dioxide (Sc CO_2) based deposition of metal and metal oxide thin film is a new area of interest in microelectronics. Recently, a few studies reported Sc CO_2 assisted metal deposition at lower temperatures (~60-125°C) [1-3] compared to the high vacuum processes. All previous metal depositions in Sc CO_2 were performed in a batch process named Chemical Fluid Deposition (CFD). [1-5] In this study, we used Sc CO_2 in depositing metal oxides and gate metals by atomic layer deposition (ALD) process. ALD is a cyclic deposition process where the deposition surface undergoes sequential exposure to the reactants.[6-9] The self-limiting adsorption of precursors on the substrate and subsequent reaction limit the film growth in monolayer/sub-monolayer thickness in each cycle.[7] Therefore, ALD allows tuning the thickness of a highly conformal ultra-thin film in case of restricted surface geometries.[7-9] Low process temperature, better film quality, multilayer processing ability, and uniformity of film on large area are the other advantages of ALD.[7] We anticipate added benefits to ALD by incorporating the beneficial aspects of Sc CO_2 in the process.

$ScCO_2$ based deposition can overcome certain limitation of conventional high vacuum and solvent based deposition processes because of its unique physiochemical properties.[1-3, 5] The density of Sc CO_2 can approach or exceed that of a liquid while its diffusivity lies in between a gas and a liquid.[1, 3, 5] The high density of Sc CO_2 facilitates

dissolution of a broad range of metal organic species which overcomes the volatility constraint of many precursors in high vacuum processes.[1-5] Also the high diffusivity, low viscosity and zero surface tension of Sc CO_2 eliminate the mass transport constraint [1-5] observed in other solvent based techniques such as electroplating and electroless deposition. The high solvation energy of Sc CO_2 can be a substitute of part of the heat energy in thermally activated surface reactions. Effective use of solvation energy in metal deposition is evident from electroplating and electroless processes[12], which involve low-temperature deposition in a liquid medium. The high density and low mass transport resistance of Sc CO_2 can also facilitate the removal of reaction by products from the deposition surface which can ensure enhanced film purity.[1-3, 5]

In this study, we demonstrated cyclic deposition of aluminum oxide (Al_2O_3), palladium (Pd) and ruthenium oxide (RuO_x) film with a Sc CO_2 based ALD system. From microelectronics point of view, Al_2O_3 is important as a high k dielectric material.[10, 13, 15] Pd is important as a contact material in integrated circuits[2] while RuO_x is a promising candidate for future gate electrode applications.[16]

In our experiments, we chose metal organic precursors as the metal source because they are soluble in Sc CO_2 medium. We established linear growth of Al_2O_3 film with the number of deposition cycles. The dependence of qualitative Pd and RuO_x film thickness on deposition cycle was established. For RuO_x deposition, different surface morphology was observed for different number of deposition cycles. Chemical states of Al_2O_3 and Pd films were analyzed using X-ray Photoelectron Spectroscopy (XPS).

3.2 EXPERIMENTAL METHOD

The depositions were carried out in a home built hot-wall, stainless steel high-pressure reaction cell (internal volume 21.19 cm^3) shown schematically in figure 3.1. Two sapphire windows were used as view ports at the two ends of the reaction cell. A bigger high-pressure cell (~100 ml) was used as the precursor premix cell where the precursors were dissolved and stored in supercritical carbon dioxide for subsequent use during the experiment. Before each experiment, the cleaned premix cell was flushed with CO_2, and approximately 20-30 mg of precursor was loaded into the cell through one of its side ports. The premix cell was then pressurized with CO_2 at 1200-1500 psi and heated to 70-80°C. After reaching the set point temperature of the premix cell, ~30 minutes was allowed to ensure maximum dissolution of the precursor in the Sc CO_2. An ISCO 260D syringe pump was used to compress and deliver the carbon dioxide at the required pressure. High-pressure stainless steel tubing was used to make the CO_2 flow-connections, and high-pressure valves (max rated pressure ~15000 psi) were used to regulate the CO_2 flow. Resistive heaters with feedback control were used to maintain the temperature of the reaction cell within ±1°C of the set point value. The lines used to deliver the precursor were sometimes heated to prevent condensation and clogging.

The films were deposited on native oxide or chemical oxide on Si(100). Substrates with native oxide were prepared by JTB cleaning [JTB-100 Baker clean (5 minutes), deionized water rinse (10 minutes), and nitrogen-blow dry]. Chemically oxidized surfaces were prepared as described elsewhere[14] and dried with nitrogen flow.

At the beginning of the process, the cleaned reaction cell was heated to 40-50˚C. The samples were placed inside the cell, the windows were closed and the cell was flushed thoroughly with CO_2 for 1 or 2 minutes. The reaction cell was then pressurized above the critical pressure of CO_2 and heated to reach the set point temperature. After the temperature of the reaction cell equilibrated to the set point, the pressure inside the cell was adjusted to the set point value.

Precursors for deposition included aluminum acetylacetonate (99%) ($Al(acac)_3$) [$Al(CH_3COCHCOCH_3)_3$], aluminum hexafluoroacetylacetonate (min. 98%) ($Al(hfac)_3$) [$Al(CF_3COCHCOCF_3)_3$] and bis(cyclopentadienyl)ruthenium (99%, 99.9%-Ru) (Ruthenocene) [$(C_5H_5)_2Ru$], purchased from Strem Chemicals. Palladium (II) hexafluoroacetylacetonate ($Pd(hfac)_2$) [$(C_4HF_6O)_2Pd$] was obtained from Sigma Aldrich. All precursors were used as received. The fluorinated precursors, $Al(hfac)_3$ and $Pd(hfac)_2$ were stored in a well sealed desiccator to prevent any reaction with outside air or moisture.

The experiments were carried out in ABAB cycles as in a typical atomic layer deposition process.[15] A small amount of precursor solution (A) was injected from the premix cell to the pressurized reaction cell such that the pressure inside the reaction cell goes up by 30-50 psi. In case of the fluorinated precursors, the approximate concentration of solution injected from the premix cell was 0.05-0.1wt%. The concentrations of non-fluorinated precursors correspond to their solubility in Sc CO_2 at the pre-mix cell temperature. After the needed exposure of samples to the precursor (varies with experiments, from 30 seconds to 3 minutes) the reaction cell was vented and then flushed with liquid/supercritical CO_2 to remove the remaining precursor including any weakly adsorbed on the deposition surface. The purged CO_2 from the reaction cell was filtered in an activated charcoal bed before

venting out to the outside air. The reaction cell was then re-pressurized to the needed pressure with Sc CO_2. An oxidizing or a reducing agent (B) was confined inside a fixed length of the depressurized high-pressure tubing and subsequently driven into the reaction cell with high pressure CO_2 flow. For aluminum oxide deposition, 0.2-0.4 ml of liquid oxidizer (30% aqueous solution of H_2O_2 or 50% tert-butyl peracetate (TBP) in mineral spirits) was injected in each cycle. For ruthenium deposition, H_2O_2 solution was used in the same quantity. For palladium deposition, ultra high purity H_2 (99.999%) was used as the reducing agent. In every case, the molar quantity of the injected oxidant/reductant was hundreds of times higher than that needed for stoichiometric reaction since only a minute quantity of adsorbed precursor took part in the reaction. After the reaction (1-3 minutes depending on the experiments) the reaction cell was vented and then flushed with liquid/supercritical carbon dioxide to remove the reaction byproducts from the cell volume and from the deposition surface. After a complete AB cycle, the reaction cell was re-pressurized with Sc CO_2 for the next cycle.

On an average it took ~20 minutes to complete a full deposition cycle. The manual operation of the high pressure valves lead to uncertainty in regulating precursor and CO_2 flow. Imperfect sealing of the reaction cell and the degraded high-pressure valves often caused pressure variation inside the reaction cell, occasionally as high as a few hundreds of psi. Experimental difficulties often impeded the injection of the same volume of liquid oxidant in every cycle.

Deposited films were analyzed by ellipsometry, X-ray photoelectron spectroscopy (XPS), Auger electron spectroscopy (AES) and atomic force microscopy (AFM). A Rudolf ellipsometer (632.8 nm, 70˚ fixed angle) was used to measure the oxide thickness. XPS was

conducted using a Riber LAS3000 (MAC2 analyzer, Mg Kα hv=1253.6 eV, non-monochromatic X-ray source) at 75º take-off-angle with 0.1eV step size. A Physical Electronics Model 3017 AES subsystem with a Model 15-155A cylindrical mirror analyzer was used for the AES measurement. AES data were collected with samples normal to the analyzer with an acceleration voltage of 5 KV. A DI3000 AFM with silicon tip (Veeco Nanoprobe, Model No. OTESPA) was used in tapping mode to measure the surface roughness of the deposited films.

3.3 RESULTS AND DISCUSSION

A true atomic layer deposition process possesses two essential criteria, first the adsorption of the precursor should be self-limiting on the deposition surface and second, the film growth should proceed in a linear fashion with cycle number. Due to the self-saturating nature of ALD, film growth takes place in sub-monolayer level in each cycle. Previous studies reported 0.9-1.2 Å/cycle growth of ALD Al_2O_3 from $Al(CH_3)_3$ and water.[9-11]

In our study, we did several ALD depositions of Al_2O_3 from Al $(hfac)_3$ and H_2O_2 at fixed temperature (100°C) and pressure (~2000 psi). Figure 3.2 represents the ellipsometry data for Al_2O_3 films deposited from these experiments. Each data point was obtained by taking an arithmetic average of the film thicknesses measured on one or more samples with the same number of deposition cycles. Thickness values were taken from 3-7 measurements on each sample. The figure shows fairly linear growth of Al_2O_3 although the high growth rate indicates CVD type growth rather than a true self-limiting ALD. We noticed a significant effect of $Al(hfac)_3$ exposure time and sample orientation inside the reaction cell on the deposition rate. For the same process conditions, an increase in precursor exposure time from 30 seconds to 3 minutes showed almost a four times increase in film growth rate (2.13 and

8.44 Å respectively). When the samples were placed on a horizontal sample holder, it showed a 5.61 Å/cycle growth rate instead of 2.13 Å/cycle for the same precursor exposure time (30 seconds). In case of the sample holder, the deposition surface (un-scribed surface of the silicon substrate) was always faced upward and the precursor could flow from the precursor-inlet to the deposition surface without any mass transfer constraint. When the samples were placed without the holder, the deposition surface was placed down-faced and the other surface was directly exposed to the precursor flow. Precursor flow in the later case was restricted by the tortuous flow path from the precursor-inlet to the deposition surface and also by the narrower spacing between the down-faced deposition surface and the reactor-wall. It is to be mentioned that when the sample holder was not used, the samples sometimes changed their position due to any abrupt pressure rise inside the reaction cell while pressurizing with CO_2.

Figure 3.3 shows the AFM image of an Al_2O_3 film deposited in 23 cycles from $Al(hfac)_3$ and H_2O_2 at 100°C. The AFM scan length is 1 μm and the gray scale spans 100 Å dark to light. Each unit in z-direction corresponds to 50 nm. The RMS value for the film surface was ±2.3 nm against the film thickness of 117 Å, which is order of magnitude higher than typical ALD Al_2O_3 surface roughness. In literature, ±3Å RMS value against a 560 Å of ALD Al_2O_3 has been reported.[13]

We introduced three different sets of precursors for cyclic deposition of aluminum oxide: $Al(hfac)_3$-H_2O_2, $Al(acac)_3$-H_2O_2, and $Al(acac)_3$ – tert-butyl peracetate (TBP). In our previous work, we presented a detailed discussion on comparative film compositions for the later two sets of precursors.[17]

The $Al(hfac)_3$-H_2O_2 based depositions were carried out at 100ºC and ~2000 psi with a 3 minutes of precursor exposure/cycle. Both of the $Al(acac)_3$-H_2O_2 and $Al(acac)_3$-TBP systems were carried out at 120ºC, ~1600 psi, and 1 minute of precursor exposure/cycle. The above three systems are represented in table 3.2 in terms of their cycle number, film thicknesses and O to Al-atomic ratio (from XPS analysis). In case of $Al(acac)_3$-TBP, the poor Al-content in the deposited film (O:Al ~14) can be related to the limited oxidizing ability of TBP compared to H_2O_2. A slower growth rate was also observed in this case [35 Å/12-cycles from $Al(acac)_3$-TBP against 40 Å/9-cycles from $Al(acac)_3$- H_2O_2] . The $Al(hfac)_3$-H_2O_2 system showed a better Al-incorporation in deposited films. For this system, the 10, 20 and 30 cycles of deposition show O to Al atomic ratio, 4.9, 2.8, and 3.1 respectively. In all cases higher O:Al values were obtained compared to the stoichiometric value, 1.5 in pure Al_2O_3. The sources of this excess oxygen are the different oxygen containing species other than Al_2O_3 in deposited films, which will be evident from subsequent discussions.

Figure 3.4 represents the detailed XP-spectra for I. Al2p, II. O1s, and III. C1s peaks for films deposited from the above three sets of precursors. In the figure, (a), (b) and (c) stand for $Al(hfac)_3$-H_2O_2, $Al(acac)_3$-H_2O_2 and $Al(acac)_3$-TBP respectively. The broad distributions of Al2p (figure 3.4 I) and O1s (figure 3.4 II) signals reveal that Al is in multiple oxidation states in the deposited films. The literature binding energy for Al2p in Al_2O_3, $Al(OH)_3$, and AlO(OH) are 74.6[24], 74.3-75.9[25,26], 76.7[25] eV respectively while those for O1s are 531.4[28], 531.53[18], and 531.5[26] eV respectively. By considering both Al2p and O1s peaks, we conclude that Al_2O_3 and $Al(OH)_3$ are the dominant aluminum-species in films deposited from $Al(hfac)_3$-H_2O_2 and $Al(acac)_3$-H_2O_2 while, in case of $Al(acac)_3$-H_2O_2, the prime sources of aluminum is attributed to AlO(OH).

Aluminum oxide films deposited from the three different sets of precursors show substantial carbon contamination as evident from figure 3.4 III. The prime source of carbon was attributed to the adventitious carbon (C1s at 284.8 eV[18]). When H_2O_2 was used as the oxidant, a second peak was observed near the higher binding energy side of the C1s peak [figure 3.4 III (a) and (b)] which was attributed to the presence of carbonate species (289.4eV[19]) in the film. When TBP was used as the oxidant, no such peak was observed [figure 3.4 III. (c)]. The reasoning behind the carbonate formation is the water used in the 30% H_2O_2 solution. Acidic nature of water-Sc CO_2 mixture and carbonic acid formation due to water-Sc CO_2 interaction has been reported elsewhere.[20] Formation of carbonate can be due to the reaction between carbonic acid and deposited aluminum oxide. Also 'monodentated' bicarbonate and 'bidentated' carbonates are expected from adsorption of CO_2 on hydroxylated Al_2O_3 surface. [21,22,23]

Despite different temperature, pressure and precursor exposure time, it was a reasonable guess that the different reactant species were the key determinants of film composition in the above three cases.

Palladium films obtained from our experiments were poorly adhesive to native oxide. Similar results were reported by Watkins and his co-authors in their work.[2] Although bright and reflective films were obtained from the experiments, most of the films were washed away from the sample surface while cleaning in ethanol in a bath sonicator at room temperature. The survey spectra (figure not included) did not show any noticeable fluorine peak although we speculated small amount of fluorine contamination in the film by analyzing the detailed C1s spectra (figure 3.5a). The C1s peak was set at 284.8 eV since the adventitious carbon was taken as the prime source of carbon contamination. The asymmetric

broadening of the C1s peak to its higher binding energy side indicates the presence of C-O, C=O, CF_x and CF_3 in the film. Similar results were reported by Lin et al.[30], and Senkevich et al[31] as they deposited Pd by self-reduction of $Pd(hfac)_2$ on copper and tertrasulfide self-assembled monolayer surface respectively. The broad hump around 286.5-289.5 was attributed to C-O, CF_x and C=O due to the thermal fragmentation of the original $Pd(hafc)_2$ molecule[30,31]. The small step near 292.3 eV corresponds CF_3 in an intact $Pd(hfac)_2$ molecule (after adjustment of adventitious C1s peak) as reported in literature.[30,32]

Setting the C1s peak to the adventitious carbon binding energy shifts the Pd3d peak to the literature binding energy of elemental Pd ($Pd3d_{5/2}$ at 335.5 eV[33], figure 3.5b).

The absence of fluorine peak in the survey spectra and the Pd peak at the elemental palladium indicate minute quantity of fluorine in the deposited film. The O1s signal observed at 532.8 eV (figure 3.5c) was attributed to adventitious oxygen (532.58 eV[18]), oxygen bonded to the native SiO_2 (533.2 eV[34]) and oxygen bonded to fragmented or intact precursor molecule (~532.3 eV[30]). Quantitative analysis from detailed O1s and Si2p peaks gives oxygen to silicon atomic ratio of 3.4, which also confirms the presence of excess oxygen in the deposited film.

The partial XPS survey spectra in figure 3.6 show relative Si2p and Pd 3d peaks for two different ALD runs of palladium. The ratio of signal-intensity for the two peaks confirms that the film thickness can be tuned by varying the number of deposition cycles and the precursor exposure time. The 20 cycles and three minutes $Pd(hfac)_2$ exposure/cycle gave a much thicker film (larger Pd3d to Si2p peak-height ratio) compared to a 15cycles and one minute $Pd(hfac)_2$ exposure/cycle. Although actual thickness of deposited films were not measured, the large difference in relative Pd3d/Si2p signals for a difference of only five

deposition cycles between the two samples indicates high, CVD type growth rather than self-limiting monolayer deposition. We observed the same behavior in case of ALD Al_2O_3 deposition (figure 3.2).

Figure 3.7 shows the AES survey spectra and high-resolution peak of Ru (inset) for a 10 cycle ALD of ruthenium oxide from ruthenocene and H_2O_2. Deposition was carried out on native silicon at 100°C and ~ 2000 psi. The survey spectra show substantial carbon contamination and the ruthenium peak was difficult to identify. The high resolution Ru LMM peak at 2252 eV confirmed the presence of ruthenium in the film. Also an O KLL peak was observed at 517 eV.

RuO_x was also deposited on chemically oxidized surface of Si(100) from ruthenocene and H_2O_2 at 200°C and ~1500 psi. Depositions were carried out in 08, 20, 30 and 40 cycles. In all cases, both the Ru3d (partially overlapped with C1s peak) and Ru 3p peaks are clearly identified on the survey spectra (not included in the figure). Figure 3.8 represents the detailed XP-spectra for Ru3p and Si2p peaks for the 08, 20 and 40-cycles of deposition. The figure shows an increasing ratio of Ru3p to Si2p intensities as the number of deposition cycle increases, which indicates growing film thickness with number of cycles.

The AFM images of RuO_x films deposited in 08, 20 and 30 -cycles (as mentioned earlier) are represented in figure 3.9a, 3.9b and 3.9c respectively. In all cases, the AFM scan length of 1 μm, and the gray scale spanned 100 Å from dark to light. Figure 8a shows fairly uniform deposition of oval shaped islands, which takes columnar shape as the number of deposition cycle increases (3.9b and 3.9c). RMS values for the 8, 20 and 40-cycle depositions

are ±1.06, ±1.38 and ±3.43 nm respectively. Increased surface roughness and change in surface morphology argues for a non-ideal ALD growth.

3.4 CONCLUSION

Table 1 represents a summary of this work and its results. In this work, we introduced a new approach in metal and metal oxide deposition by developing a supercritical carbon dioxide based ALD process. Aluminum oxide, palladium and ruthenium oxide films were deposited from different metal organic precursors in supercritical carbon dioxide solution. The Al_2O_3 film, deposited from $Al(hfac)_3$-H_2O_2 showed linear growth with ALD cycle number. Longer precursor exposure time led to CVD type growth of Al_2O_3 rather than monolayer formation. Deposited Al_2O_3 films from different precursors were composed of a mixture of different aluminum-oxygen compounds such as Al_2O_3, $Al(OH)_3$, AlO(OH) and carbonate species. We speculated CVD type growth of palladium from $Pd(hfac)_2$-H_2 with trace extent of ligand and precursor derived contamination. The RuO_x film showed different surface morphology at different deposition cycles. The overall result from this work confirms that the process can tune the thickness of the film although it is unable to control the growth in atomic scale.

3.5 ACKNOWLEDGEMENTS

Financial support from NSF (Grant# CTS- 0304296) and the NSF Science and Technology Center for Environmentally Responsible Solvents and Processes is gratefully acknowledged. We would also like to acknowledge Ke Wang for assistance with the sc CO_2 experimental set up and Ruben Carbonell for helpful discussions.

3.6 REFERENCES

1. James J. Watkins, Jason M. Blackburn and Thomas J. McCarthy, "Chemical Fluid Deposition: Reactive Deposition of Platinum Metal from Carbon Dioxide Solution, *Chemistry of Materials* **11**, 213-215 (1999)

2. Jason M. Blackburn, David P. Long, and James J. Watkins, "Reactive Deposition of Conformal Palladium Films from Supercritical Carbon Dioxide Solution", *Chemistry of Materials*, **12,** 2625-2631 (2000)

3. Albertina Cabanas, David P. Long, and James J. Watkins, "Deposition of Gold Films and Nanostructures from Supercritical Carbon Dioxide", *Chemistry of Materials* **16**, 2028-2033(2004)

4. Ephrem T. Hunde and James J. Watkins, "Reactive Deposition of Cobalt and Nickel Films from Their Metallocenes in Supercritical Carbon Dioxide Solution", *Chemistry of Materials* **16**, 498-503 (2004)

5. Albertina Cabanas, Xiaoying Shan, and James J. Watkins, Alcohol-Assisted Deposition of Copper Films from Supercritical Carbon Dioxide, *Chemistry of Materials* **15**, 2910-2916 (2003)

6. Markku Leskela, Mikko Ritala, "Atomic layer deposition (ALD): from precursors to tin film structures", *Thin Solid Films* **409**, 138-146(2002)

7. Mikko Ritala, and Markku Leskela, "Atomic layer epitaxy-a valuable tool for nanotechnology?", *Nanotechnology* **10**, 19-24(1999)

8. Mathew D. Halls and Krishnan Raghavachari, "Atomic Layer Growth Reactions of Al2O3 on Si(100)-2×1", *Journal of Physical Chemistry B* ***108***, 4058-4062(2004)

9. Riikka L. Puurunen, "Growth Per Cycle in Atomic Layer Deposition: Real Application Examples of a Theoretical Model", *Chemical Vapor Deposition* **9**, 327-332 (2003)

10. Y. Chang, F. Ducroquet, E. Gautier, O. Renault, J. Legrand, J.F. Damlencourt, F. Martin, " Surface preparation and post thermal treatment effects on interface propertires of thin Al_2O_3 films deposited by ALD", *Microelectronic Engineering* **72**, 326-331 (2004)

11. Jeffrey R. Wank, Steven M. Geroge, and Alan W. Weimer, "Coating Fine Nickel Particles with Al_2O_3 Utilizing and Atomic Layer Deposition-Fluidized Bed Reactor (ALD-FBR)", *Journal of the American Ceramic Society* **87**, 762-765 (2004)

12. N. Petrov, U. Sverdlov, and Y. Shacham-Diamond, "Electrochemical Study of the Electrolesss Deposition of Co(P) and Co(W, P) alloys", *Journal of the Electrochemical Society* **149**, C187-C-194(2002)

13. A. W. Ott, J.W. Klaus, J.M. Johnson, S.M. George, "Al_2O_3 thin film growth on Si(100) using binary reaction sequence chemistry", *Thin Solid Films* **292**, 135-144(1997)

14. M. L. Green, M.-Y. Ho, B. Busch, G.D. Wilk, and T. Sorsch, "Nucleation and growth of atomic layer deposited HfO_2 gate dielectric layers on chemical oxide (Si-O-H) and thermal oxide (SiO_2 or Si-O-N)", *Journal of Applied Physics* **92**, 7168-7174 (2002)

15. A. W. Ott, K.C. McCarley, J.W. Klaus, J.D. Way, S.M. George, "Atomic layer controlled deposition of Al_2O_3 films using binary reaction sequence chemistry", *Applied Surface Science* **107**, 128-136(1996)

16. K. Frohlich, K. Husekova, D. Machajdik, J.C. Hooker, N. Perez, M. Fanciulli, S. Ferrari, C. Wiemer, A. Dimoulas, G. Vellianitis, F. Roozeboom, "Ru and RuO_2 gate electrodes for advanced CMOS technology", *Materials Science and Engineering B* **109**, 117-121(2004)

17. Theodosia Gougousi, Dipak Barua, Erin D. Young, Gregory N. Parsons, "Metal-oxide thin films deposited from metal organic precursors in supercritical CO_2 solutions" Manuscript in preparation.

18. C. D. Wagner, D.E. Passoja, H.F. Hillery, T.G. Kinisky, H.A. Six, W.T. jansen, J.A. Taylor, "Auger and photoelectron line energy relationship in aluminu,-oxygen and silicon-oxygen compounds" *Journal of Vacuum Science and Technology* **21**, 933-944(1982)

19. J. S. Hammond, J. W. Holubka, J. E. DeVries and R.A. Dickie, "The Application of X-Ray photo-electron Spectroscopy to a Study of Interfacial Composition in Corrosion-induced Paint De-adhesion", *Corrosion Science* **21**, 239-253(1981)

20. Karen L. Toews, Robert M. Shroll, and C.M. Wai, "pH-Defining Equillibrium between Water and Supercritical CO2. Influence on SFE of Organics and Metal Chelates", *Analytical Chemistry* **67**, 4040-4043(1995)

21. Maurizio Casarin, Daniele Falcomer, Antonella Glisenti, and Andrea Vittadini, "Experimental and Theoretical Study of the Interaction of CO_2 with α-Al_2O_3", *Inorganic Chemistry* **42**, 436-445 (2003)

22. Maurizio Casarin, Daniele Falcomer, Andrea Vittadini, " A theoretical study of the interaction of CO_2 with hydroxylated α-alumina", *Surafce Science* 566-568, 890-894(2004)

23. Hideto Tsuji, Akie Okamura-Yoshida, Tetsuya Shishido, and Hideshi Hattori, "Dynamic Behavior of Carbonate Species on Metal Oxide Surface: Oxygen Scrambling between Adsorbed Carbon Dioxide and Oxide Surface" *Langmuir* **19**, 8793-8800 (2003)

24. K. Arata, M. Hino, "Solid Catalyst Treated with Anion.18.Benzoylation of Toluene with Benzoyl Chloride and Benzoic Anhydride Catalyzed by Solid Superacid of Sulfate-Supported Alumina" *Appl. Catalysis* **59**, 197 (1990)

25. J.R. Lindsay, H.J. Rose, W.E. Swartz, P.H. Watts, K.A. Rayburn, "X-ray photoelectron spectra of aluminum oxides-structural effects on chemical-shift", *Applied Spectroscopy* **27**, 1-5(1973)

26. J.A. Taylor, "An XPS study of the oxidation of alas thin-films grown by MBE", *Journal of Vacuum Science & Technology* **20**, 751-755(1982)

27. Jaebum Kim, Kuntal Chakrabarti, Jinho Lee, Ki-Young Oh and Chongmu Lee,"Effects of ozone as an oxygen source on the properties of the Al_2O_3 thin films prepared by atomic layer deposition", *Materials Chemistry and Physics* **78** 733–738 (2003)

28. E. Paparazzo, "XPS analysis of iron aluminum-oxide systems, *Applied Surface Science* **25**, 1-12(1986)

29. G. Bandoli, D. Barreca, E. Brescacin, G.A. Rizzi and E. Tondello, Chemical Vapor Deposition **2**, 238(1996)

30. Wenbin Lin, Benjamin C. Wiegand, Ralph G. Nuzzo, and Gregory S. Girolami, "Mechanistic Studies of Palladium Thin Film Growth from Palladium (II) β-Diketonates. 1. Spectroscopic Studies of the Reactions of

Bis(hedafluoroacetylacetonato) palladium(II) on Copper Surface, *Journal of American Chemical Society* **118**, 5977-5987 (1996)

31. Jay J. Senkevich, Fu Tang, Diana Rogers, Jason T. Drotar, Christopher Jezewski, William A. Landford, Gwo-ching Wang, and Toh-Ming Lu, "Substrate-Independent Palladium Atomic Layer Deposition", *Chemical Vapor Deposition* **9**, 258-264(2003)

32. Jay J. Senkevich, Christopher J. Mitchell, G.-R. Yang, T.-M. Lu, "Reduced sulfur-terminated silanes to promote the interaction of palladium(II) hexafluoroacetylacetonate with dielectric surfaces", *Colloids and Surfaces A*: *Physicochem. Eng. Aspects* **221**, 29-37(2003)

33. Gobind Kumar, J.R. Blackburn, R.G. Albridge, W.E. Moddeman, and M.M. Jones, "Photoelectron Spectroscopy of Coordination Compounds. II. Palladium Complexes", *Inorganic Chemistry* **11**, 296-300(1972)

34. Taylor JA, Lancaster GM, Rabalais JW, "Chemical-reactions of N-2+Ion-beams with group-IV elements and their oxides", *Journal of Electron Spectroscopy and related phenomena* **13**, 435-444(1978)

Table 3.1 List of metal and metal oxide films, precursors, experimental conditions and net results

Material deposited	Precursor	Solubility in Sc CO_2	Oxidizer/Reducer	Temperature Studied	Substrate	Comments
Al_2O_3	$Al(hfac)_3$	Very good	30% H_2O_2 in H_2O	100°C	Native SiO_2	Better Al content, multilayer growth/cycle
	$Al(acac)_3$	Poor	30% H_2O_2 in H_2O	120°C	Native SiO_2	Less Al content, multilayer growth /cycle
	$Al(acac)_3$	Poor	50% tert-butyl peracetate in mineral spirits	120°C	Native SiO_2	Small amount of Al, multilayer growth/cycle
Palladium, Pd	$Pd(hfac)_2$	Very good	Hydrogen	70 and 80° C	Native SiO_2	Bright, yellow color film, poor adhesiveness, trace extent of F contamination, multilayer growth/cycle
Ruthenium Oxide (RuO_x)	Ruthenocene	Poor	30% H_2O_2 in H_2O	100°C	Native SiO_2	High C contamination, Barely detectable Ruthenium peak (AES)
				200°C	Chemically grown oxide	Increasing growth of film thickness (XPS), and increasing surface roughness (AFM) with number of ALD cycles

Table 3.2 Number of deposition cycle, corresponding film thickness, and oxygen to aluminum atomic ratio in deposited films from three different sets of precursors.

	$Al(acac)_3$-H_2O_2	$Al(acac)_3$-TBP	$Al(hfac)_3$-H_2O_2		
No. of Cycles	9	12	10	20	30
Thickness (Å)	40	35	96	147	275
O:Al (atomic ratio)	5.6	14	4.9	2.8	3.1

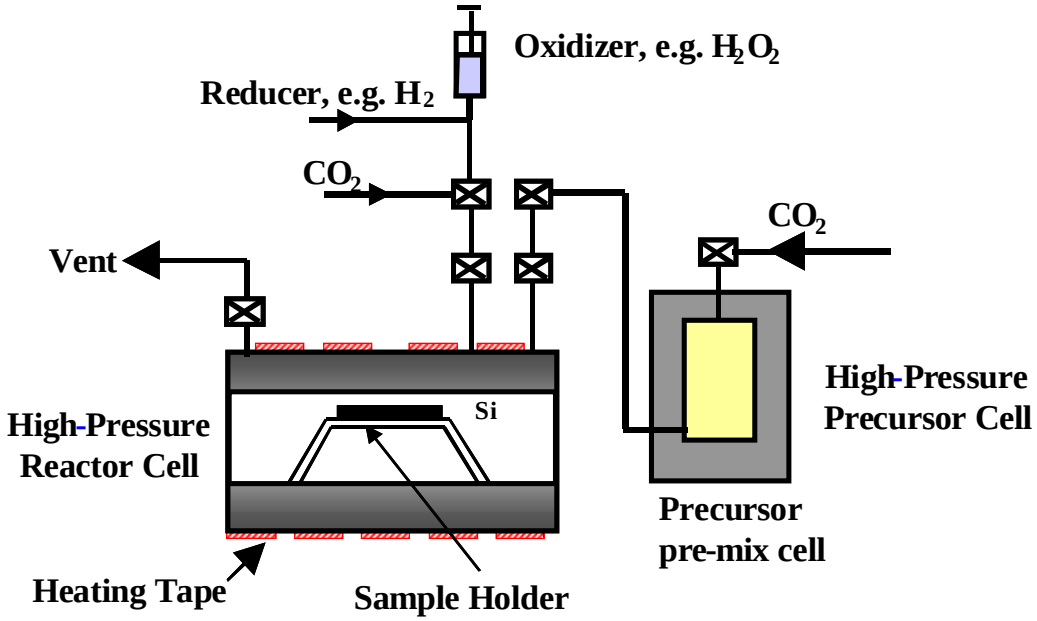

Figure 3.1 Schematic diagram of the experimental set-up

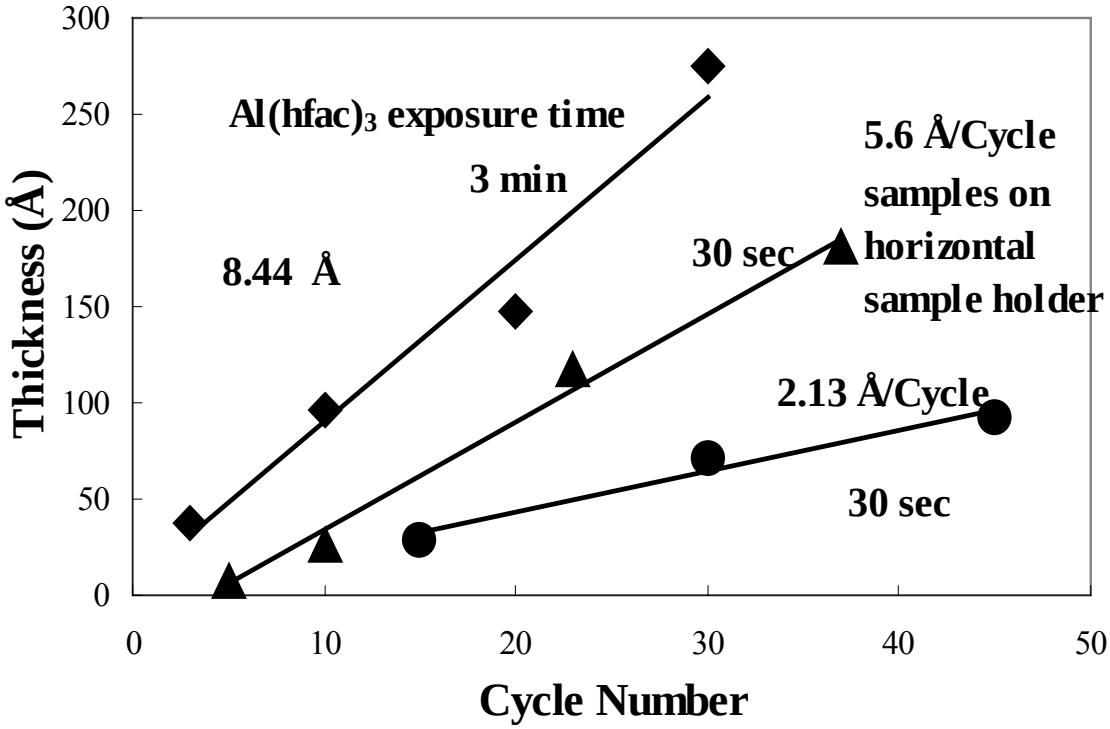

Figure 3.2 Ellipsometric thickness data for Al-based film deposited from $Al(hfac)_3$-H_2O_2 at 100°C and ~2000 psi on Si(100) with native oxide. Figure shows linear growth behavior. Longer precursor time shows high rate of film growth. For same precursor exposure time (30 seconds), different growth rates are observed for two different sample orientations.

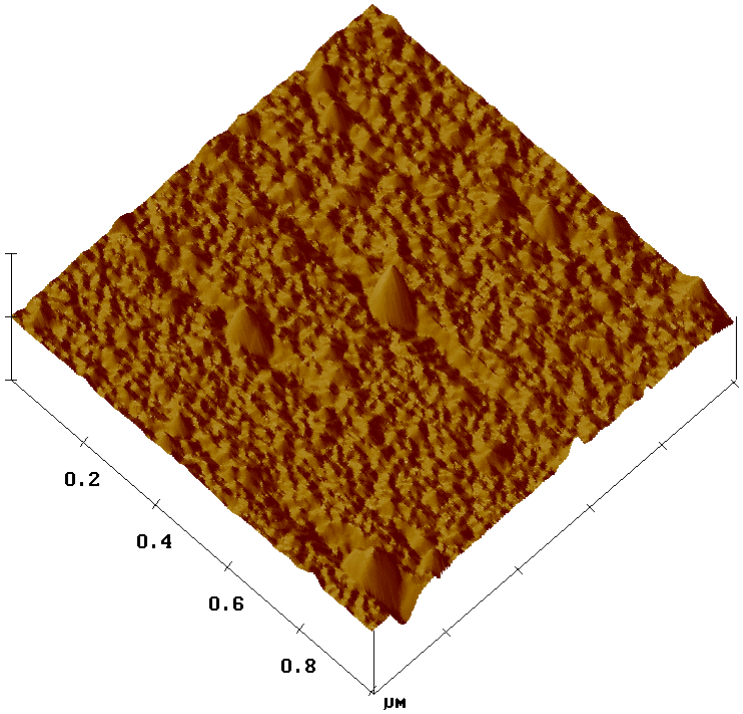

Figure 3.3 AFM image of Al-based film deposited in 23 cycles from $Al(hfac)_3$-H_2O_2, at 100°C and ~2000 psi. JTB treated native Si(100) is used as the substrate. The RMS value for the film is ±2.3 nm while the ellipsometric thickness is 117 Å. The gray scale of this image spans 100 Å from dark to light and each unit in the z-direction corresponds to 50 nm.

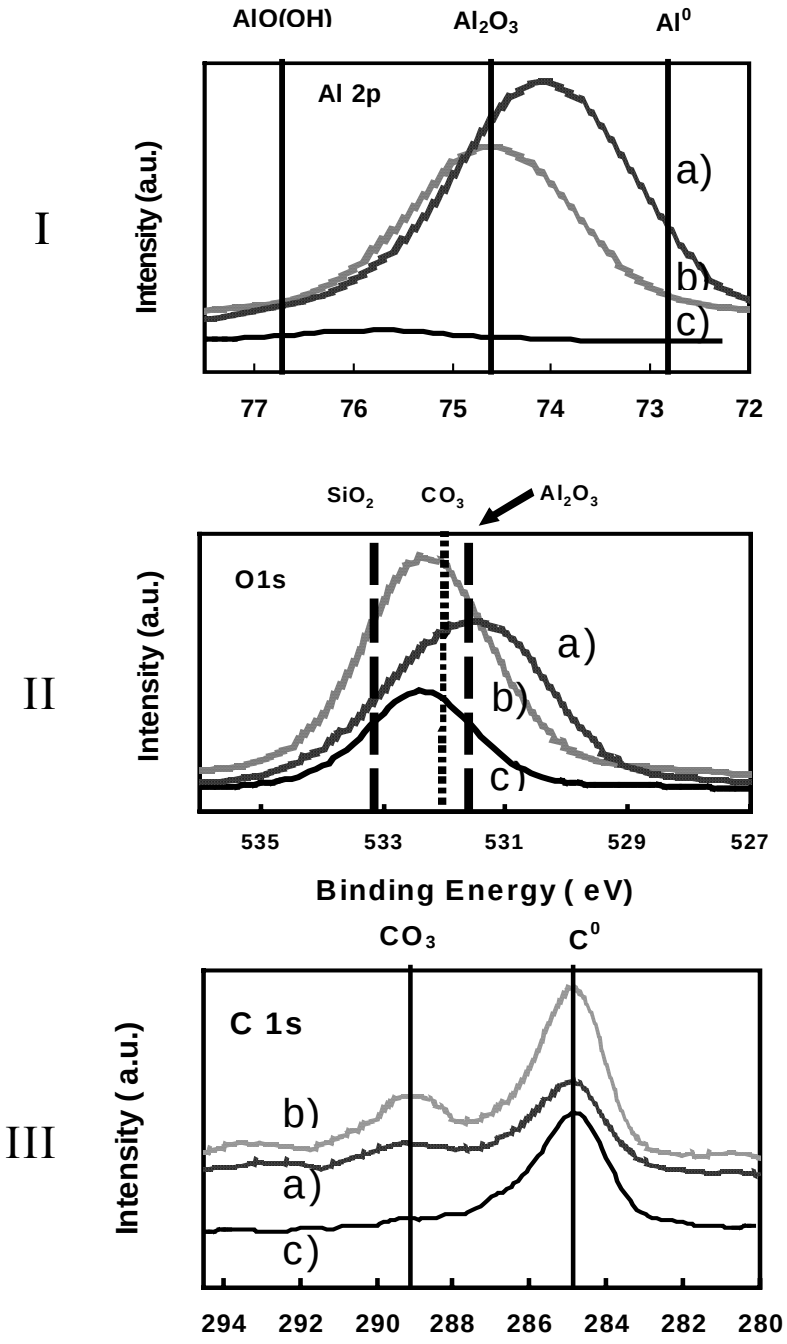

Figure 3.4 High-resolution XPS peaks for I. Al 2p, II. O 1s, and III. C 1s deposited from a)$Al(hfac)_3$-H_2O_2 at 100°C,~2000 psi, b)$Al(acac)_3$-H_2O_2 at 120°C, ~1600 psi, and c) $Al(acac)_3$-TBP at 120°C and ~1600 psi. Native Si(100) is used as the substrate. Comparative chemical states are evaluated from the relative peak positions for the different sets of precursors.

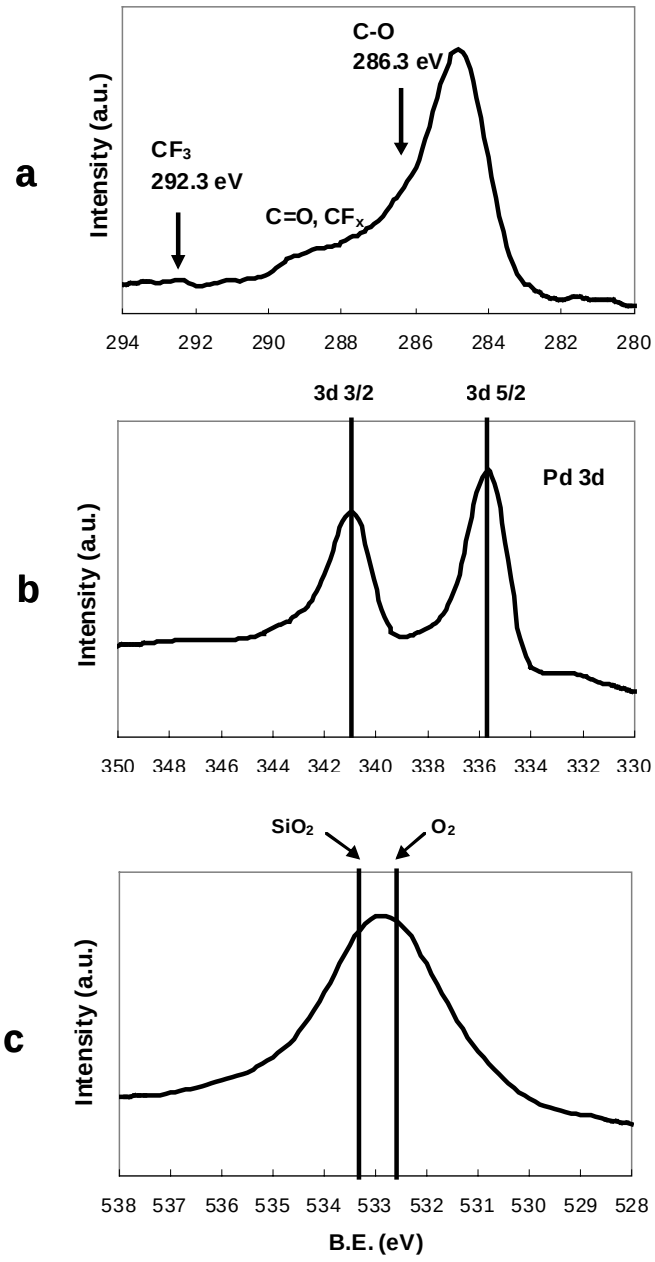

Figure 3.5 High resolution XP-Spectra for a) C1s, b) Pd 2p,and c) O1s for palladium film deposited from $Pd(hfac)_2$-H_2 in 20 cycles. Native Si(100) is used as the substrate. Deposition temperature is 70°C and pressure ~2000 psi. Ligand and precursor derived contamination from fluorine, carbon and oxygen is anticipated.

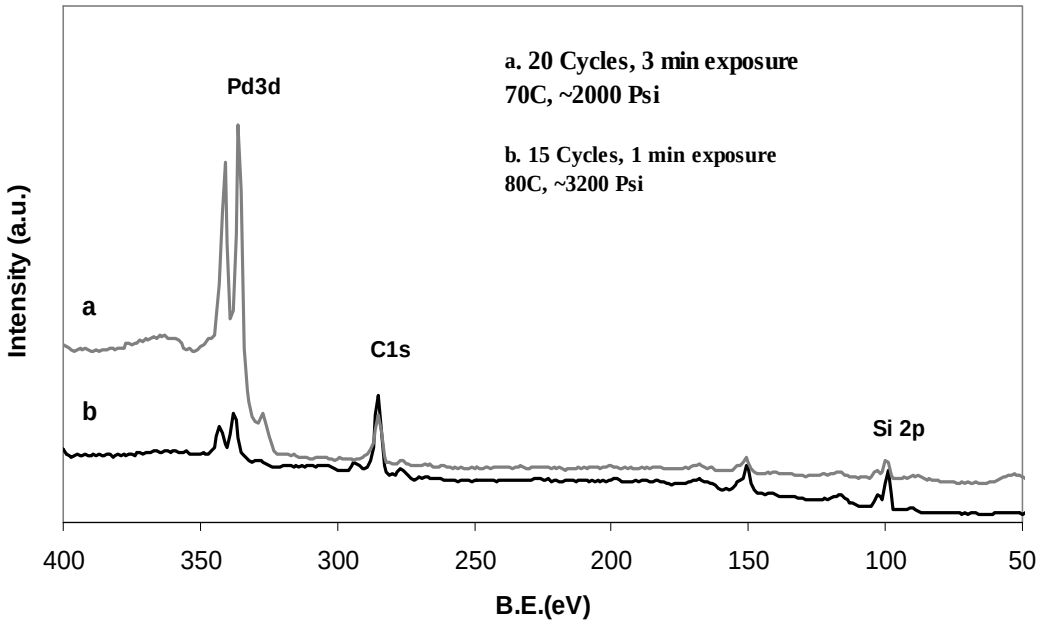

Figure 3.6 Comparative XPS peaks for Pd3d and Si 2p.Palladium film is deposited from $Pd(hfac)_2$-H_2 in different two different number of cycles. Si(100) with native oxide is used as the substrate. The large difference in Pd3d to Si2p peak-height ratio in two cases indicates multilayer film growth in each cycle.

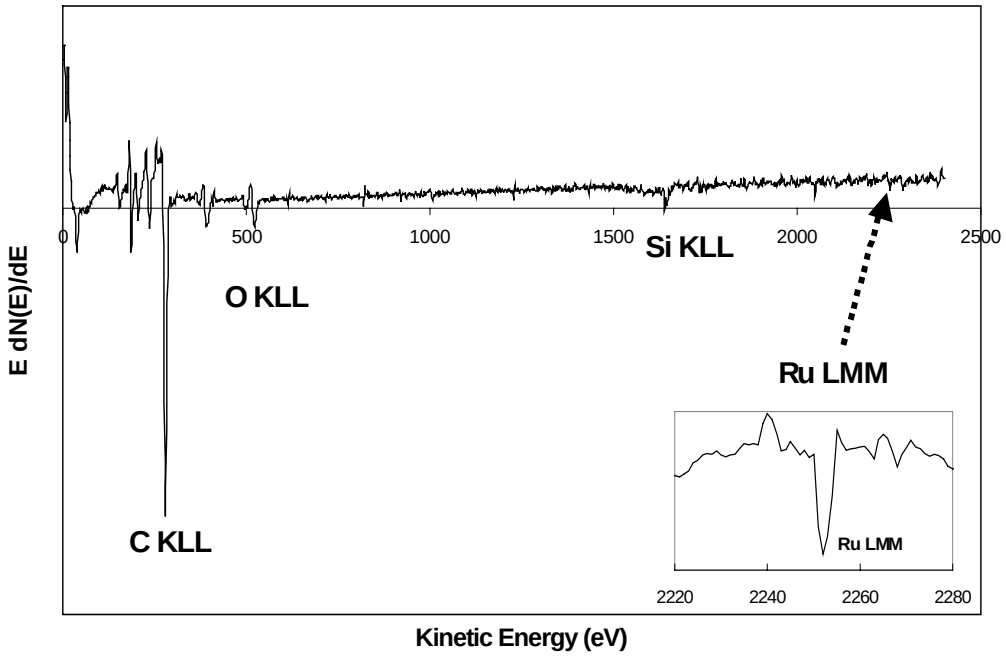

Figure 3.7 AES survey spectra for RuO_x film deposited from ruthenocene ($RuCp_2$) and H_2O_2 in 10 cycles. Reaction temperature is 100° C and pressure ~2000 psi. Si(100) with native oxide is used for deposition. The inset shows high- resolution peak for Ru LMM.

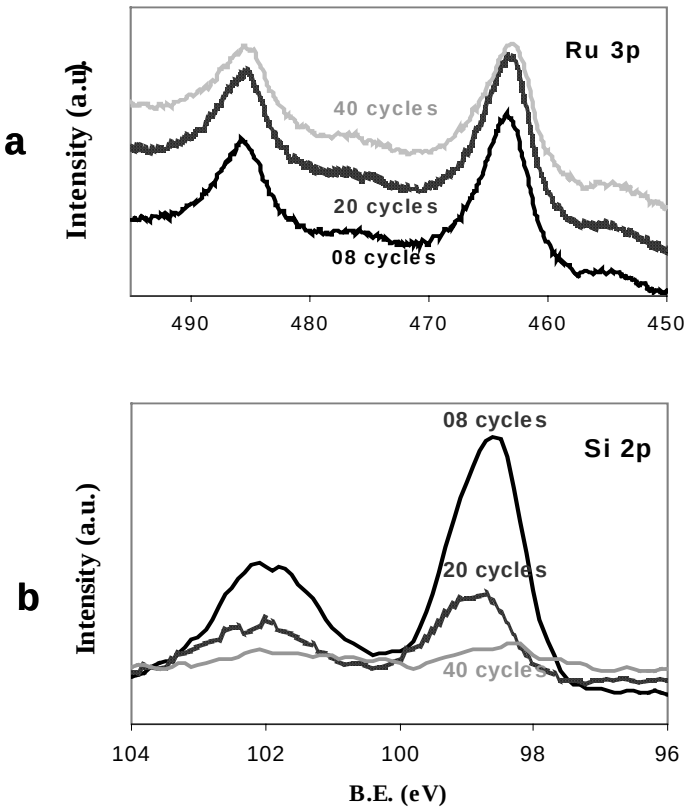

Figure 3.8 High resolution XP-spectra showing a) Ru3p and b) Si 2p peaks for the RuOx films deposited on chemically oxidized surface of Si(100) at 200°C and ~1500 psi. The attenuating intensity of Si 2p signal indicates growing film thickness with increasing number of deposition cycle.

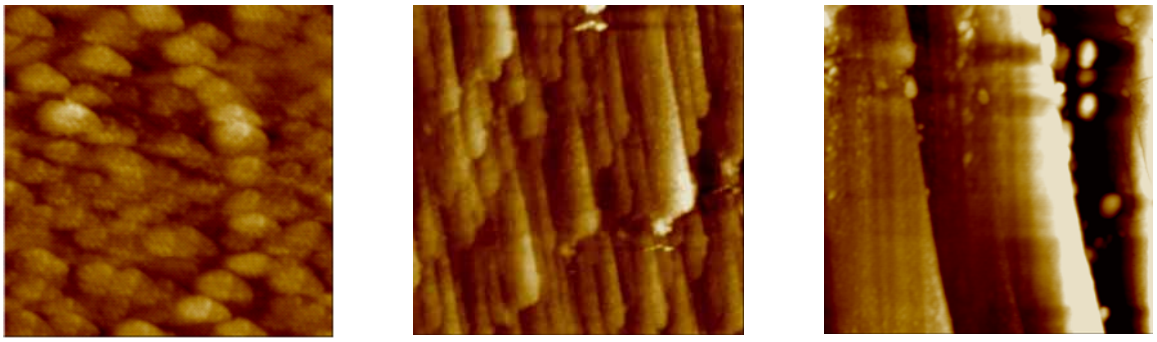

Figure 3.9 AFM images of Ru/RuOx film deposited from $RuCp_2$ and H_2O_2 at 200°C and ~1500 psi: a) 8 cycles, b)20 cycles, and c)30 cycles. Chemically oxidized Si(100) was used for the deposition. Figure shows increasing surface roughness with increasing number of deposition cycles. Change in interface morphology indicates non-ideal ALD growth.

CHAPTER FOUR

4.1 WORK SUMMARY

In quest of a new process for metal and metal oxide thin film deposition, the supercritical carbon dioxide based deposition process has been chosen to dig out its unexplored possibilities. In all cases, a low deposition temperature (70-200ºC) is adopted to verify the claim that Sc CO_2 based deposition can be performed at much lower temperatures compared to the high vacuum processes. Metal organic precursors are chosen because of their high solubility in supercritical carbon dioxide and to facilitate the low temperature deposition. Experiments are carried out in two processes: chemical fluid deposition (CFD) and atomic layer deposition (ALD)

In this work, new sets of materials are established for metal and metal oxide deposition. Deposited metal oxides include aluminum oxide, zirconium oxide, manganese oxide, ruthenium oxide and yttrium oxide, and metals include palladium and ruthenium. Detailed compositional analyses of the deposited films are performed in light of XPS and FTIR measurements. Different oxidation states of metals are observed in metal oxide films. Also carbonates species and ligand-derived contaminations are observed depending on the precursors and other chemicals used in the process. Electrical characterization of aluminum oxide is performed by capacitance-voltage measurement. Good electrical properties are established from the measured data.

The ALD experiments confirm a predictable and controllable growth rate of aluminum oxide film although high growth rate invalidate an ideal ALD process in this case.

The surface morphology of metal -oxide films are analyzed by atomic force microscopy (AFM). High surface roughness and changing interface morphology confirms that the cyclic process adopted was not an ideal ALD.

In this study, we showed the first deposition of metal oxides in supercritical carbon dioxide. Also we established the supercritical carbon dioxide based atomic layer deposition process for the first time. Although the quality of deposited films were not up to expectation in many cases, and the ALD was not satisfied completely in terms of its basic criteria, a more rigorous study can lead to process optimizations and other important findings which can eventually make this process a parallel one with currently established high vacuum processes.

4.2 FUTURE WORK

The metal and metal-oxide films, deposited in this study, often showed undesired chemical composition and contamination. Results indicate the need for an optimized process in order to ensure better quality films. The next focus of this study will be on studying the effect of different process parameters, specifically process temperature, pressure, and precursor concentration on the film quality and film growth. A cold-wall reactor approach will be better suited for this purpose instead of the currently used hot- wall, high-pressure cell.

The next step will be to deposit gate metals on high-k dielectric layer. Focus will be on evaluating the electrical properties of devices formed thereby.

The other goal of this study will be to deposit metal films in selective deposition approach. Recently our research group showed selective deposition of ruthenium on octadecyltrichlorosilane (OTS) patterned silicon in a high vacuum ALD process. The same

approach will be taken in this Sc CO_2 based system. Palladium and ruthenium are of primary interests in this regard.